J. Space Weather Space Clim. 2018, 8, A27

https://doi.org/10.1051/swsc/2018006

SWSC

Available online at:
www.swsc-journal.org

RESEARCH ARTICLE

Multi-station investigation of spread F over Europe during low to high solar activity

Krishnendu Sekhar Paul[1,2,*], Haris Haralambous[2], Christina Oikonomou[3], Ashik Paul[1], Anna Belehaki[4], Tsagouri Ioanna[4], Daniel Kouba[5] and Dalia Buresova[5]

[1] Institute of Radio Physics and Electronics, University of Calcutta, Calcutta, India
[2] Frederick University, Nicosia, Cyprus
[3] Frederick Research Center, Nicosia, Cyprus
[4] National observatory of Athens, Athens, Greece
[5] Institute of Atmospheric Physics, Prague, Czech Republic

Received 5 October 2017 / Accepted 24 January 2018

Abstract – Spread F is an ionospheric phenomenon which has been reported and analyzed extensively over equatorial regions on the basis of the *Rayleigh-Taylor* (R-T) instability. It has also been investigated over midlatitude regions, mostly over the Southern Hemisphere with its generation attributed to the *Perkins instability* mechanism. Over midlatitudes it has also been correlated with geomagnetic storms through the excitation of travelling ionospheric disturbances (TIDs) and subsequent F region uplifts. The present study deals with the occurrence rate of nighttime spread F events and their diurnal, seasonal and solar cycle variation observed over three stations in the European longitude sector namely Nicosia (geographic Lat: 35.29 °N, Long: 33.38 °E geographic: geomagnetic Lat: 29.38 °N), Athens (geographic Lat: 37.98 °N, Long: 23.73 °E geographic: geomagnetic Lat: 34.61 °N) and Pruhonice (geographic Lat: 50.05 °N, Long: 14.41 °E geographic: geomagnetic Lat: 47.7 °N) during 2009, 2015 and 2016 encompassing periods of low, medium and high solar activity, respectively. The latitudinal and longitudinal variation of spread F occurrence was examined by considering different instability triggering mechanisms and precursors which past literature identified as critical to the generation of spread F events. The main findings of this investigation is an inverse solar cycle and annual temporal dependence of the spread F occurrence rate and a different dominant spread F type between low and high European midlatitudes.

Keywords: nighttime midlatitude ionosphere over Europe / effects of solar activity over spread F occurrence / longitudinal and latitudinal dependence of spread F occurrence

1 Introduction

After seven decades of extensive research, some irregular behavior of midlatitude ionosphere is still not fully clear to the scientific community. Range or frequency spread of the ionospheric F layer (spread F) is sudden distribution of plasma structures at F-region due to the generation of field aligned irregularities with different scale sizes (Herman, 1966) or the tilted ionospheric surface produced by travelling ionospheric disturbances (TIDs). King (1970) observed spread F development over several midlatitude stations as large scale tilts of the bottomside F layer isodensity contours. He suggested that rather than small scale irregularities, these large tilted patterns are primarily responsible for spread F generation in the nighttime midlatitude ionosphere. Space weather refers to adverse conditions on the Sun, the solar wind, and in the Earth's magnetosphere, the ionosphere, and the thermosphere. One of the important outcomes of a space weather event is related to generation of ionospheric irregularities. Excellent review articles on ionospheric F region irregularities are available (Fejer & Kelley, 1980). Scattering of signals from these irregularities embedded in the ionosphere are obtained in the form of spread F on radar maps and ionograms (Woodman & La Hoz, 1976; Fejer & Kelley, 1980; Bowman, 1990). Plasma depletions were first observed by the polar orbiting OGO-6 satellite (Hanson & Sanatani, 1973). The irregularities, in the form of depletions, manifest as deep bite-outs in in-situ density plots (Kelley et al., 1976; McClure et al., 1977), and cause scintillations in transionospheric satellite links (Basu & Basu, 1976; Basu & Whitney, 1983). Airglow observations with all-sky cameras establish that the irregularity clouds become narrower with latitude on both sides of the magnetic equator

*Corresponding author: krish6372@gmail.com

(Weber et al., 1980). Several studies have been reported in literature devoted to plasma dynamics to determine the origin and the triggering mechanisms of midlatitude spread F (Fejer & Kelley, 1980; Bowman, 1990; Hajkowicz, 2007). Nevertheless, the role of neutral drivers responsible for plasma instability at nighttime midlatitude ionosphere are still unresolved issues in between sporadic E (Es) layers, TIDs and plasma density irregularities associated with *Perkins instability*. Perkins (1973) demonstrated the *Perkins instability* as widely used equilibrium where the nighttime ionospheric spread F is supported by $E \times B$ drifts is unstable if with a supporting eastward field a north-south electric field component exists. The occurrence of nighttime spread F irregularities with various scale sizes (from less than a meter to several kilometers) was first observed by Booker & Wells (1938). Later, various different instruments such as ground-based ionosondes, coherent and incoherent scatter radars, MU radars, satellite-borne top-side sounders, HF Doppler radars, GNSS satellite receivers and *in-situ* measurements (Fejer & Kelley, 1980; Basu & Basu, 1985; Kelly, 1989; Fukao et al., 1991; Mathews et al., 2001; Swartz et al., 2002; Chandra et al., 2003; Xiao et al., 2007) were used to reveal the morphological features of spread F occurrence including its long term characteristics such as its dependence on solar activity, diurnal, seasonal and latitude/longitude variations (Rastogi, 1977; Bowman, 1984, 1986, 1988a, 1988b, 1990; Huang et al., 2011). These morphological features of spread F still need the attention of the scientific community, as spread F significantly complicates ionospheric predictions.

During daytime, midlatitude plasma distribution is mainly controlled by diffusion, neutral wind shear and strong polarized electric fields. The poleward neutral wind drives the plasma density towards lower altitudes whereas the opposite effects are caused by meridional wind. During nighttime, reduced plasma density limits the interaction with neutral wind, which in turn gives rise to nighttime plasma motion in the F region of midlatitude ionosphere. For different geomagnetic configurations in the midlatitude region, during post sunset hours, the *Raleigh-Tailor* (R-T) instability is not fully effective, as it was observed in the equatorial region (Rastogi & Klobuchar, 1990). The *Perkins instability* has been proposed as an alternative driving mechanism for the formation of midlatitude irregularities (Perkins, 1973). Kelly (1989) pointed out that plasma instability such as R-T *instability* might affect spread F development along with the *Perkins instability.* Huang et al. (1994) have established that for the lower growth rate of *Perkins instability* due to saturation, the gravity wave plays a major role as a seeding mechanism for the generation of midlatitude nighttime spread F. Also gravity waves enhance the instability growth rate significantly unless limited by third or fourth order non-linearities. Thus, a seeding of the *Perkins instability* by gravity waves may be observed, which in turn initiates the plasma instability at midlatitudes. Huang et al. (1994) showed that during post sunset hours, the *Perkins instability* at the bottom of the F layer could be initiated by gravity waves and develop into large amplitude oscillations. The enhanced amplitude of gravity waves can accelerate the growth rate of the instabilities and induce irregularities in the nighttime midlatitude F layer. The correlation between gravity waves as a driving agent with the nighttime midlatitude spread F were also studied (Xiao et al., 2009). Earle et al. (2010) suggested that midlatitude spread F development is usually related with wave driven meso-scale (10–100 km) plasma distributions. The signature of TIDs associated with gravity waves could be observed prior to the onset of midlatitude spread F (Bowman, 1990). Lambert (1988) performed statistical analysis of midlatitude spread F occurrence for two regions of South Africa to investigate the effects of short period TID patterns over nighttime spread F events during a minimum solar activity year. Jayachandran et al. (1987) observed equatorial MS-TIDs during spread F events. They noted a significant fluctuation in the drift velocity component (V_Z) several minutes before the onset of spread F. Haldoupis et al. (2003) studied the occurrence of unstable midlatitude Es layer patches from Crete, Greece (geomagnetic Lat: 37.98 °N, Long: 23.73 °E geographic: geomagnetic Lat: 34.6 °N) and thereby tried to establish a link between midlatitude spread F and Es layer. They suggested the existence of electric field inside the Es layer, which in turn transports plasma density horizontally by means of local neutral winds and high Hall-to-Pederson conductivity ratios at different altitudes of the E region. This locally generated polarized electric field inside the Es layer can simply align the magnetic field lines to the bottom of F region and trigger the instability mechanism of spread F generation. Singleton (1968) had presented the temporal variation of spread F occurrence throughout half a solar cycle over a network of stations (around 36 °S to 76 °N) over American longitudinal sector. He suggested that during low solar activity, spread F would diffuse towards higher latitudes from lower latitude regions, whereas during high solar activity, high occurrence of spread F events may be observed frequently at higher latitudes. He also observed a clear difference between spread F distribution during low and high solar activity periods in the vicinity of 50° (N and S) latitude.

Tsunoda & White (1981) in their empirical study found that large scale wave structures (LSWS) that appear at the bottom of the F layer as isodensity contours of plasma distribution may serve as a precursor for the development of nighttime spread F. McNicol et al. (1956) also spotted some echoes accompanied by spread F events observed below the critical frequency of the F layer during nighttime and they termed these echoes as 'satellite' traces (STs). They characterized these traces with mean lifetime of 50 min at a maximum occurrence rate during winter from Brisbane (Lat: 27.5 °S, Lon: 153 °E geographic; magnetic dip. 35.1 °S). However the most advanced sensors used for detecting irregular plasma distributions are not able to identify LSWS due to their spatial structure and insignificant zonal drifts (Tsunoda & White, 1981). Most suitable data, from which the distinct features of LSWS could be tracked, are obtained from incoherent-scatter radars with a steerable beam (ALTAIR) (Tsunoda & White, 1981), or from coherent-scatter radars with multiple beams (Tsunoda & Ecklund, 2007), and total electron content (TEC) derived from observations of low inclination orbital satellites (Tsunoda & Towle, 1979), or newly data obtained from vertical and oblique HF sounding with a network of synchronize digisondes (Verhulst et al., 2017).

In the midlatitude ionosphere, the occurrence of nighttime spread F is frequent, when compared with both high (≥60°) and equatorial (0°–±30°) latitude regions. Shimazaki (1962) studied the global latitudinal distribution of spread F. It was observed that the occurrence of equatorial spread F is limited to

Table 1. Geographic and Geomagnetic locations of the stations used for the study.

Stations	Longitude (°E)	Latitude (°N)	Geomagnetic DIP (°N)
Nicosia (Cyprus)	33.38	35.19	29.38
Athens (Greece)	23.73	37.98	34.61
Pruhonice (Czech Republic)	14.41	50.05	47.70

20° latitude with maximum probability of occurrence at the equator, whereas the occurrence probability of high latitude spread F increases from 40° to 60° and maximizes above 60°. He also noted that high latitude spread F is more severe than equatorial spread F. The occurrence of spread F also exhibits a significant latitudinal and longitudinal variability both in equatorial and midlatitude regions (Singleton, 1968; Batista et al., 1986; Abdu et al., 1992; Bowman, 2001; Mwene et al., 2004; Earle et al., 2006; Bhaneja et al., 2009). Singleton (1968) observed clear latitudinal variations in spread F occurrence. He investigated seasonal and solar activity effects on spread F development with respect to latitude variation. Hajkowicz (2007) noted a sharp gradient of spread F occurrence along equatorward direction at the latitude range of 52° to 48°S. Huang et al. (2009) presented the longitudinal aspect on the occurrence of spread F using the IRI model which, unfortunately, provides lower accuracy over African and Indian low latitude stations due to limited data sources. Igarashi & Kato (1993) have carried out similar studies over different Asian longitudes. However, it is important to study the effect of longitudinal variability of spread F in conjunction to various mechanisms related with spread F development.

The present study aims to investigate the temporal variation of spread F statistics perhaps for the first time over low-to-midlatitude transition region covering the eastern Mediterranean longitude sector by employing Digisonde measurements at Nicosia (Cyprus) (geographic Lat: 35.19 °N, Long: 33.38 °E geographic; Geomagnetic. dip: 29.38 °N), Athens (Greece) (geographic Lat: 37.98 °N, Long: 23.73 °E geographic; Geomagnetic. dip: 34.61 °N) and Pruhonice (Czech Republic) (geographic Lat: 50.05 °N, Long: 14.41 °E geographic; Geomagnetic. dip: 47.70 °N) during the years of 2009, 2015 and 2016. It is necessary to mention that 2009 was an extremely low solar activity year, whereas 2015 was relatively high and 2016 a moderate solar activity year. The two stations Nicosia and Athens lie almost along the same geographic latitude (the latitudinal difference between these two stations is ~2.5°), whereas Pruhonice is situated further north. The three stations have significant differences in longitude as well. New observations of spread F and ionospheric signatures of relevant mechanisms that have been previously reported as instability drivers in the nighttime F layer over various time scales (e.g. diurnal, seasonal variations, solar activity etc.) in conjunction with latitudinal/longitudinal spread F characteristics are presented in this study. To study the effect of TIDs, the variation in vertical TEC from GPS was examined from three IGS stations namely NICO, NOAA and G0PE which are situated adjacent to Nicosia, Athens and Pruhonice ionosonde stations, respectively. The fluctuations observed in the vertical plasma drift velocity prior to onset of spread F signifies the presence of TID patterns in the nighttime F layer. The present study deals with such fluctuations as measured by Digisondes. A case study of 3rd August 2015 has been considered in order to investigate a nighttime midlatitude spread F event observed simultaneously over the three stations.

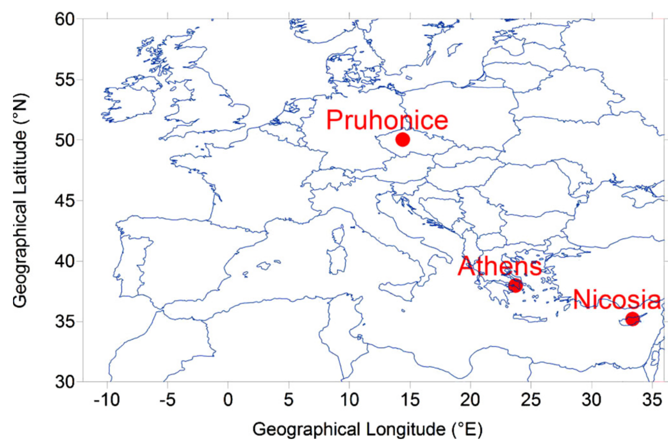

Fig. 1. Geographical locations of Nicosia (Cyprus), Athens (Greece) and Pruhonice (Czech Republic) at the European continent.

2 Data and methodology

A multi station investigation was conducted during 2009, 2015 and 2016 to study morphological characteristics of European post sunset midlatitude ionosphere involving European ionospheric stations at (1) Nicosia, Cyprus (geographic Lat: 35.19 °N, Long: 33.38 °E geographic; Geomagnetic. dip: 29.38 °N) (2) Athens, Greece (geographic Lat: 37.98 °N, Long: 23.73 °E geographic; Geomagnetic. dip: 34.61 °N) and (3) Pruhonice, Czech Republic (geographic Lat: 50.05 °N, Long: 14.41 °E geographic; Geomagnetic. dip: 47.70 °N).

Figure 1 shows the locations of the stations involved in the analysis and Table 1 gives the corresponding geographical and geomagnetic coordinates. In 2009, the yearly average sunspot number was 4.8 whereas the corresponding mean value of 10.7 cm solar flux (F10.7) was 70.5. In 2015, the yearly mean of sunspot number and F10.7 were 69.8 and 117.7 respectively. Similarly in 2016, the corresponding sunspot number and F10.7 were 39.8 and 88.8, respectively. Therefore data have been used corresponding to low, high and moderate solar activity levels.

The Nicosia digital Ionosonde DPS-4D (Reinisch et al., 2009) is fully operational since 2008 except for a few operational gaps. This state-of-art ionosonde performs auto-scaling of all important characteristics in real time. A similar state-of-art ionosonde has been operating in the National Observatory of Athens, Greece since September 2000 and was

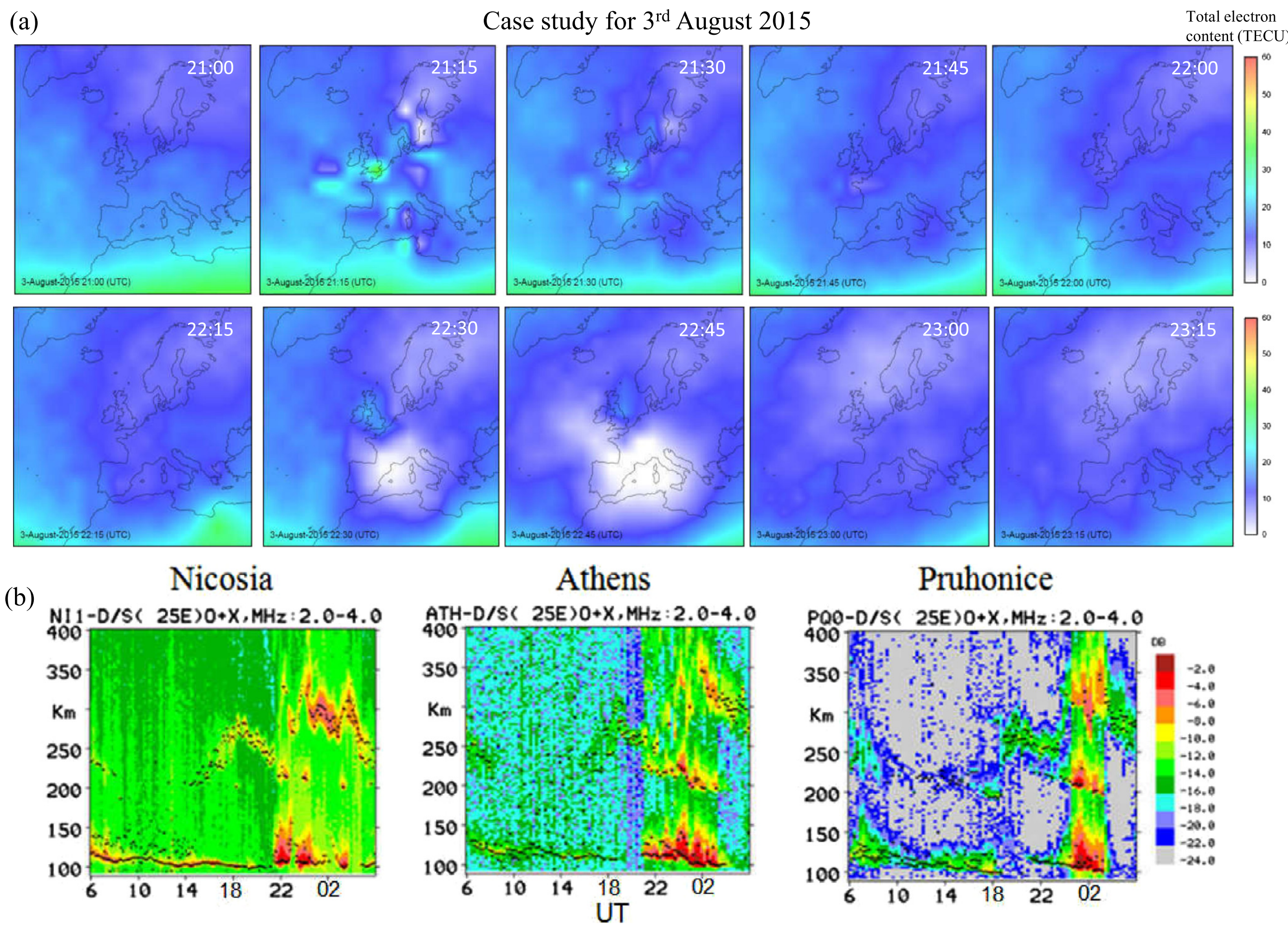

Fig. 2. Case study of 3rd August 2015 (a) plasma density distribution over the European longitude sector from 21:00 to 23:15 UT (b) individual 24-h HTI plots for Nicosia, Athens and Pruhonice.

recently upgraded to digisonde DPS-4D. Since January 2004 Digisonde DPS-4 (Beran et al., 2015) provides routine ionospheric measurements at the Pruhonice Observatory of Czech Republic every 15 min, except special campaigns with higher sampling rate. For the present study, data at 15 min resolution were used from all three stations.

To examine TID activity prior to the onset of spread F, GPS TEC measurements from IGS stations at Nicosia, Athens and Pruhonice have been extracted. Perturbed TEC data from available satellites with 30s resolution and elevation angle greater than 20° have been analyzed to identify TID signatures prior to the onset of spread F. To study the effect of TIDs more extensively, the fluctuations observed in the vertical plasma drift velocity over the three stations have been considered with a 15 min time resolution. The TID activity detected from plasma drift velocity and from GPS TEC is designated as Vz-TID and GPS-TID, respectively in the following sections.

3 Results

3.1 Case study of 3rd August 2015

One of the most severe irregularities in the nighttime midlatitude ionosphere is the sudden development of spread F at different F layer altitudes. These irregularity structures are usually associated with large scale gravity waves (Bowman, 1990), induced electromagnetic field alignment between the bottom of F layer and unstable Es layers (Tsunoda & Cosgrove, 2001; Haldoupis et al., 2003) and *gradient drift* and *Perkins instabilities* (Perkins, 1973). The 15 min maps of TEC (TECU) over the European longitude sector spanning 10 °W to 35 °E from 21:00 to 23:15 UT on August 3, 2015 are presented in Figure 2a. 3rd August 2015 was a magnetically quiet day ($Dst_{min}\sim 2nT$) at a relatively high solar activity (SSN ~ 61) phase. It can be observed that during 21:15 to 21:30 UT, the nighttime F region plasma density distribution was affected by irregularity distributions, which reappeared during 22:30 to 22:45 UT and could be related to spread F development over the European longitudes. As 3rdAugust 2015 was a magnetically quiet day, the sudden plasma depletion observed may indicate the generation of local irregularities under the influence of gravity waves which may originate from the lower atmosphere and trigger the instability at the bottom of the F layer (Huang et al., 2011).The focus of the present paper is limited to three ionosonde stations of European longitude sector, namely, Nicosia, Athens and Pruhonice. The stations at Nicosia and Athens are situated at around 35° to 37 °N latitude whereas Pruhonice is at higher latitude (~50 °N). On the 3rd

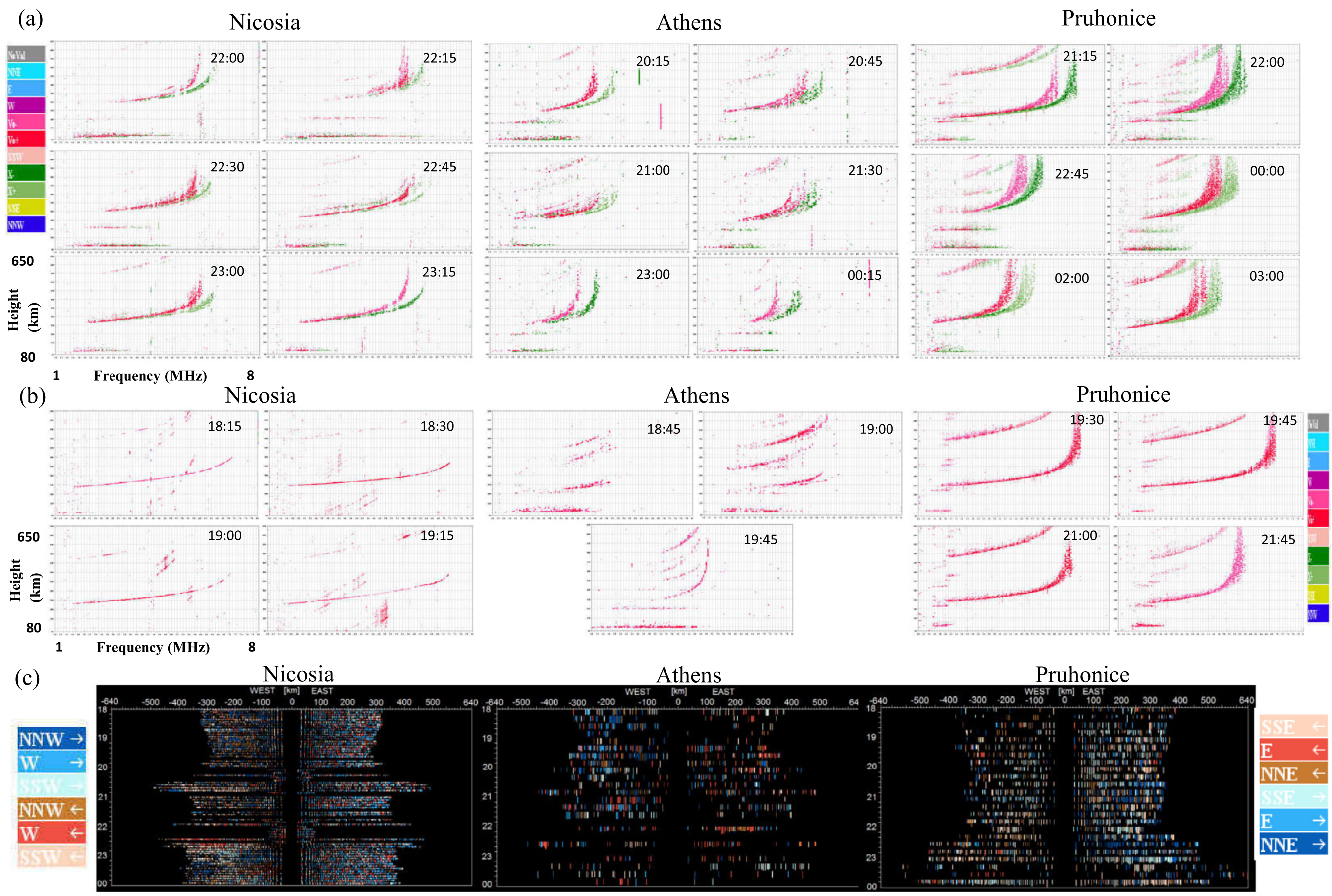

Fig. 3. Case study of 3rd August 2015 (a) Ionograms recorded by the DPS-4D Ionosonde on 3rd–4th August over Nicosia, Athens and Pruhonice (b) Nicosia, Athens and Pruhonice ionograms with LSWS traces (c) Directogram over Nicosia, Athens and Pruhonice showing echoes from off-vertical directions.

August 2015, ionosphere above all three stations was affected by irregularities almost at the same time. Efforts have been made to examine possible mechanisms that could stimulate the development of spread F.

To visualize altitude changes due to the presence of irregularities (Oikonomou et al., 2014) individual 24-h *height time intensity* (HTI) plots have been produced for each station as shown in Figure 2b. HTI technique considers an ionogram as a snapshot of reflected plasma intensity as a function of height and Digisonde operating frequency, and produces a 3D plot of reflected signal-to-noise ratio in dB as a function of height for a certain time interval. Since the present study concentrates on the development of spread F, only HTI plots with 2.0–4.0 MHz frequency bins have been considered. The color indices represent the level of carrier to noise ratio (C/N_0) of the Digisonde received signal in dB. From Figure 2b, similar F region plasma distribution patterns could be seen around 300–350 km, as well as unstable Es layers during 22:00–2:00 UT at all three stations. The evidence of electrodynamic coupling between Es with F layer (Tsunoda & Cosgrove, 2001) may indicate that possibly similar triggering mechanism was behind the instability for spread F development in this particular case.

The sequence of recorded ionograms during 20:00 UT to 3:00 UT during 3rd–4th August, 2015 at the three stations are shown in the Figure 3a. The leftmost sequence of ionograms corresponds to Nicosia, the rightmost group to Pruhonice and the middle to Athens. As it is well established that ionosonde observations are sensitive to large scale plasma density irregularities with kilometer scale size, the progressive development of spread F on the ionogram traces implies the existence of such irregularities. The overhead ordinary (O) and extra-ordinary (X) polarization traces are designated in red and green color, respectively. From the sequence of ionograms recorded above Nicosia, a certain degree of frequency spreading in both O and X polarization of 1F trace is identified during 22:15–22:45 UT as shown in Figure 2a. The phenomenon clearly demonstrates the initiation of frequency spread F (FSF). However spread F was not fully developed possibly due to the absence of sufficient plasma irregularities. In Athens, range spread F (RSF) has been observed during 20:45 to 21:30 UT and then from 23:30 to 00:15 UT. Strong Es is also visible on the ionograms. The ionograms recorded over Pruhonice exhibit severe spread F from 21:30 to 3:00 UT. From Figure 3a, it can be noted that around 21:15 UT, irregularities were observed near Pruhonice, which could have initiated the generation of large scale irregularities. Gradually under the influence of vertical plasma drifts, these irregularity structures were uplifted to higher F layer altitudes and developed into FSF through altitude modulation.

The signatures of LSWS on ionograms could be identified as STs and multi-reflected echoes (MREs), which in turn serve as precursory signatures for spread F development (Tsunoda, 2008). The hypothesis for electric field coupling between F region and strong sporadic E (Es) prior to spread F evolution, and possible effects induced by gravity wave activity (e.g. TIDs, F layer uplift, coupling between Es and F layer etc), as an external instability driver in the F region was also examined from the point of view of possible excitation of the Perkins instability growth at middle latitudes. Local generated midlatitude irregularities have been associated with the Perkins instability (Perkins, 1973).This hypothesis was further supported by studies of unstable Es layers that would electrodynamically couple to the F region and could give rise to F region instabilities faster than predicted, based on the Perkins instability mechanism (Tsunoda & Cosgrove, 2001; Haldoupis et al., 2003). Earle et al. (2006, 2008) reported LSWS acting as a decisive factor at midlatitudes in case of seeding the irregularity development at the bottom of the F layer during nighttime. The LSWS ionogram signatures indicating plasma upwelling at a distance from the ionosonde prior to the development of spread F are registered as STs and are manifested as a pattern of dynamically changing F region bottom tilt (McNicol et al., 1956; Tsunoda, 2008). These appear as additional traces above and below the F layer trace and also its higher order echoes due to successive reflection of ionosonde energy from the ground. These represent off-angle echoes from the passage of electron density gradients at a distance from overhead ionosphere which continues to observe a typical overhead echo and have also been referred to in literature as observational precursors of RSF at equatorial latitudes (Lyon et al., 1961; Rastogi, 1977; Abdu et al., 1981). Figure 3b shows examples of LSWS signatures (STs and MREs) (Tsunoda, 2008, 2009) observed prior to the onset of spread F over the three stations. It can be noted that in Athens and Pruhonice, clear signatures of STs were observed around 18:45 to 19:15 UT and 19:30 to 21:45 UT, respectively. In Athens, the development of spread F was noted almost 90 min after the last ST was observed, whereas in Pruhonice, STs were present after the development of spread F. The reason why they are more clearly identified at lower frequencies is the ionosonde antenna gain profile, which is wider at lower frequencies. MREs have been reported as an additional observational signature of LSWS signifying plasma upwelling directly over the ionosonde such that the isodensity contour geometry would favor ionospheric reflection coefficient enhancement due to the constructive interference of signals from various directions. They appear as discrete highly tilted traces compared to F region traces indicating higher order multiple F layer reflections (Tsunoda, 2009) from a concave isodensity surface which may be centered over the ionosonde. Over Nicosia, LSWS signatures (STs, MREs) were visible from 18:15 to 19:00 UT whereas F trace spreading was identified around 22:15 UT.

A directogram is a Digisonde product which provides an alternative view of plasma irregularities drifting over the station and enables visualization of the distance and direction of such oblique irregularities by suppressing vertical echoes from ionograms. In the following section, directogram plots have been employed over Nicosia, Athens and Pruhonice during 18:00 to 00:00 UT on 3rd August 2015 to reveal the presence and signatures of LSWS over the three stations in conjunction with spread F development. Figure 3c displays the directogram from evening to midnight for 3rd August 2015. The *x* axis represents the time in UT from three stations. The directogram displays the distance of the irregularities to the west and east of the Digisonde. Blue directogram traces indicate plasma drift from west to east, and shades of red are used to represent drift in the opposite direction. The irregularities start after 18:00 UT (coinciding with the appearance of STs and MREs on ionograms). The distance of the irregularities reaches up to 650 km on both eastern and western directions indicating the development of irregularities over a wide range of longitudes. Both eastward and westward intense plasma displacement was clearly observed after 20:00 UT from Nicosia but this displacement appears after 22:00 UT at Pruhonice. The directogram at Athens shows no clear plasma motion, but between 20:00 and 21:00 UT, some unclear traces were present in Figure 3c indicating vertical plasma movement.

3.2 Diurnal and seasonal variability of spread F

The diurnal and seasonal spread F occurrence for an extended time period in the European region has not been studied adequately. Deminov et al. (2009) reported seasonal variability of nighttime spread F over Moscow during 1975 to 1985. It is important to mention that 2009 was a low solar activity year whereas high and moderate solar activity corresponds to 2015 and 2016, respectively. To observe the diurnal behavior of spread F, the data (combining the starting and ending times of spread F occurrences) have been categorized into 4 seasons namely spring (March–April), summer (May–August), fall (September–October) and winter (November–February). Figure 4a–c represents the seasonal behavior of spread F duration for 2009, 2015 and 2016. The *x* axis represents the onset time of spread F between the time intervals of 16:00 UT to 06:00 UT of the next day and the y axis stands for the ending time of spread F between the time intervals of 16:00 UT to 06:00 UT of the next day. As was stated before, spread F observed in four different seasons is depicted by different colored dots. Red dots represent occurrence of spread F during spring, green dots for summer, blue for fall and yellow for winter. In Figure 4a, the number of green dots appears to be the highest followed by yellow and blue dots which signifies that over Nicosia, the occurrence of spread F maximizes during summer followed by winter and spring. A very limited number of spread F cases have been recorded during fall. Another interesting behavior that can be identified is that during winter the duration of spread F maximizes followed by summer and spring. In spring, maximum number of cases for spread F onset was observed during postmidnight periods whereas in summer and winter, the onset time is distributed all over the plot. In 2009 out of 102 spread F events, 50 were recorded during summer and 24 in winter. During 2015 out of 36 cases, 32 were noted in summer, and in 2016, out of 79 cases, 50 summer spread F cases were identified. In Athens, as is shown in Figure 4b, a significant number of spread F cases were observed during both summer and winter. During equinoxes (i.e. spring and fall) a significant number of spread F events occurred during all three years

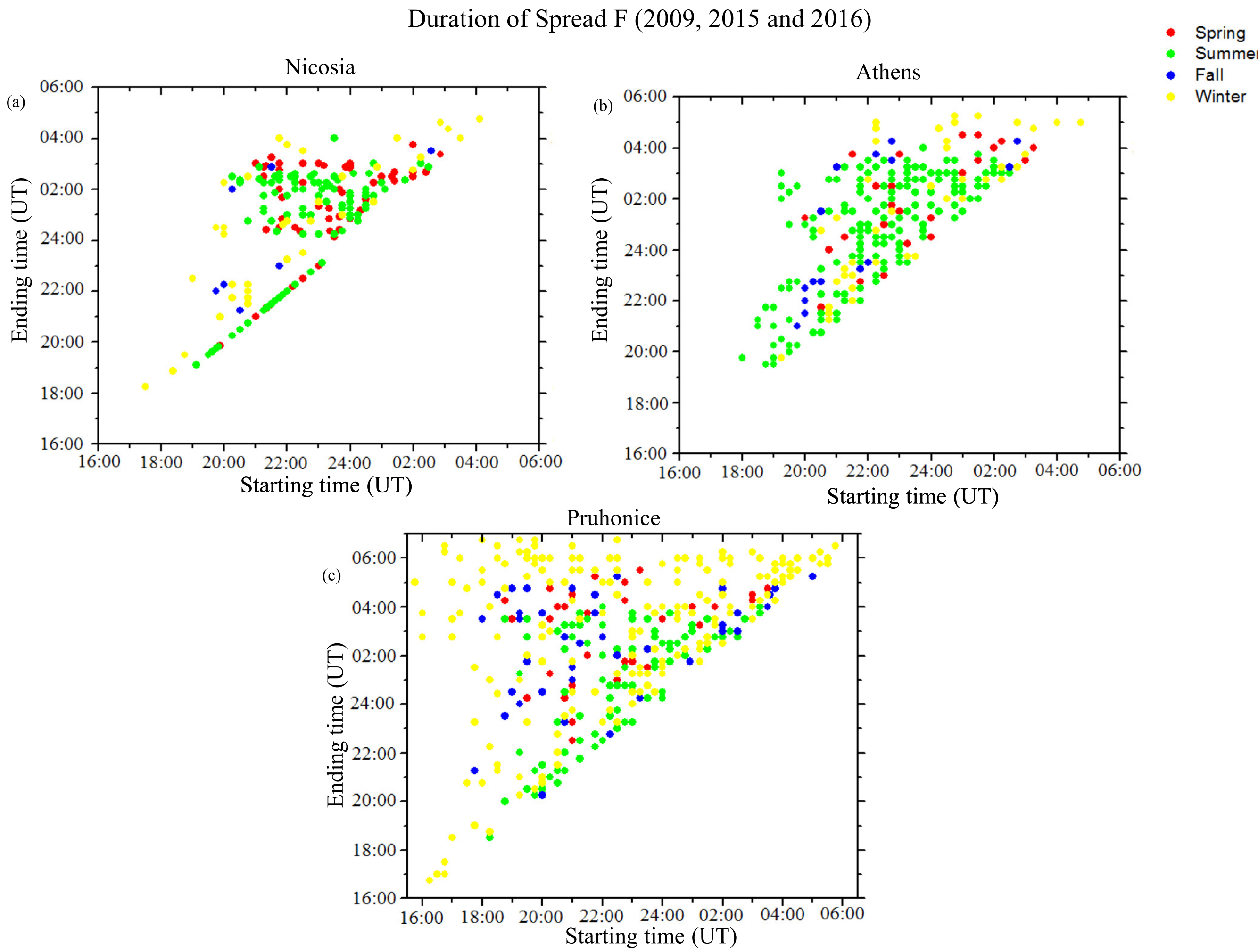

Fig. 4. Diurnal variation of spread F occurrences for different seasons observed from (a) Nicosia (b) Athens and (c) Pruhonice during 2009, 2015 and 2016.

considered. A certain threshold value (~18:00 UT) for the onset time of spread F can also be noted. The average duration of spread F peaks in winter followed by summer. Over Athens during 2009, out of 125 spread F cases, 74 were observed during summer and 22 in winter. In 2015 out of 60 cases, the number of summer spread F cases was 44 whereas in 2016 out of 86 cases, 59 were observed in summer. Thus, similar to Nicosia, the annual maximum of spread F occurrence in Athens was observed during summer followed by a secondary maximum in winter at low solar activity. Figure 4c presents the detailed description of diurnal and seasonal variability of spread F onset over Pruhonice. Over Pruhonice, the maximum number of spread F cases was observed during winter followed by summer. Deminov et al. (2009) observed the seasonal variability of spread F occurrence over Moscow which is around the same latitude as Pruhonice. During low solar activity it was observed that the maximum probability of spread F occurrence was during local midnight hours in winter. But the summer maximum of spread F events was almost absent in their findings. At high solar activity, the semiannual component of spread F occurrence was also observed during equinoxes. In equinox, for all three years, several spread F events were recorded. In Pruhonice, the maximum average duration of spread F is noted during winter followed by summer. In spring the average onset time for spread F was around 21:00 UT whereas during summer, it was around 18:00 UT. Over Pruhonice during 2009, out of 100 spread F events, 43 cases were recorded in winter and 41 cases in summer. In 2015, the number of spread F events notably increased to 155, among which 84 cases were recorded during winter with only 24 cases in summer. Finally in 2016, the total number of spread F events was 136 with 64 cases in winter and 44 cases in summer.

3.3 Effect of solar activity in spread F occurrence

Liu et al. (2006) have studied effects of solar activity over ionospheric electron density (NmF_2) from SEM/SOHO measurement over a series of stations in east Asia/Australia. They found relationship between the solar flux with the diurnal variation of ionospheric electron density. In the present study, efforts have been carried out to investigate the solar activity dependency of midlatitude ionosphere over the European longitude sector in terms of sunspot number. Figure 5a–c

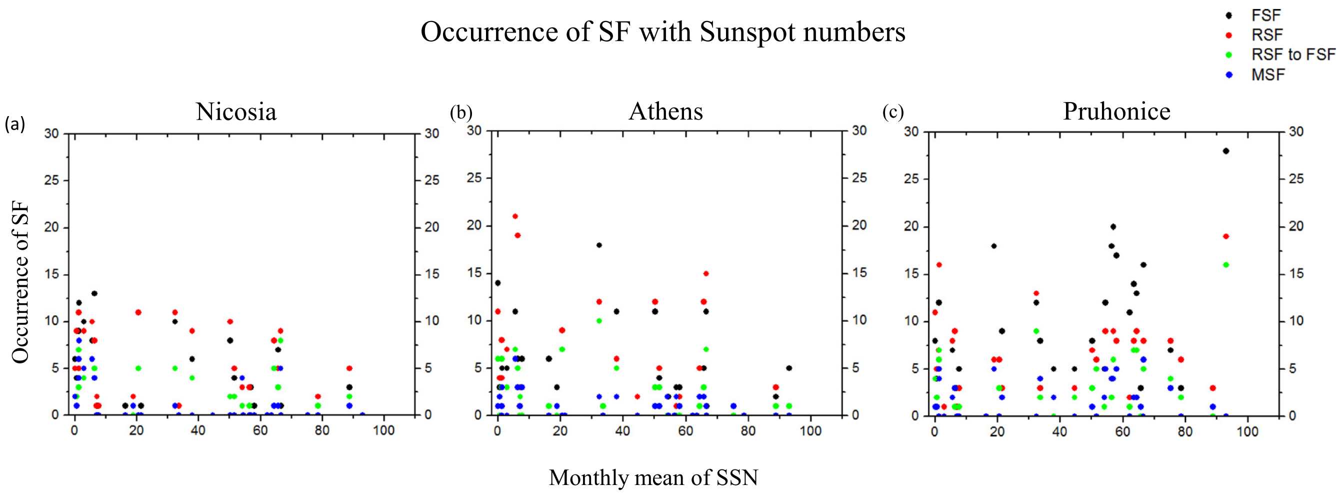

Fig. 5. Solar activity dependency of different spread F types observed from (a) Nicosia (b) Athens and (c) Pruhonice during 2009, 2015 and 2016, respectively.

presents the occurrence rate for different types of spread F with respect to the monthly mean sunspot number. The x axis shows the monthly sunspot mean whereas the monthly occurrence of spread F is shown in y axis. Four types of spread F have been observed in the recorded ionogram sequences form the three stations, namely: FSF shown by the black dots, RSF shown by red dots, range spread F evolving to RSF-to-FSF by green dots and the mixed spread F (MSF) by blue dots. In Figure 5a, the effect of solar activity on spread F occurrence over Nicosia is presented. It can be observed that the spread F occurrence maximizes for a sunspot number less than 20. A secondary maximum is also noted for FSF and RSF within a sunspot number range of 50–60. MSF is not visible frequently in this sunspot number range. In the case of Athens, a similar pattern to Nicosia can be identified. It is worth mentioning that during low solar activity, the monthly occurrence of RSF maximizes whereas during moderate solar activity, FSF is more frequent. Over Athens, moderate development of MSF has also been observed for both low and moderate solar activities. As shown in Figure 5c, it can be identified that in Pruhonice the opposite solar activity dependence is registered. Shimazaki (1962) observed a similar spread F dependence on solar activity at higher latitude regions. He reported that at locations with geomagnetic latitude over 60°, the occurrence of spread F maximizes during high solar activity. Singleton (1968) also observed intense spread F during high solar activity around 50° latitude at midlatitude ionosphere. RSF development maximizes during low solar activity at Pruhonice, but unlike Nicosia and Athens, during high solar activity, RSF was present. Since 2015 was a high solar activity year with sunspot number 60–90, a significant number of RSF cases were noted. It is necessary to point out that during January 2015 (sunspot number ~90) a high percentage of RSF were observed. FSF is dominant over midlatitudes during moderate solar activity. But for Pruhonice, the dominant occurrence of FSF persists even during high solar activity years (Singleton, 1968). Deminov et al. (2009) reported from Moscow, which is situated around the same latitude with Pruhonice, the probability of spread F occurrence during winter and fall decreases significantly with increasing solar activity. However during summer, this relation is weaker than for winter and fall. The number of RSF-to-FSF cases was also distributed almost equally over the plot at all levels of solar activity which implies that in Pruhonice, this evolution seems to be independent of solar activity.

3.4 Monthly variation of different spread F types

The occurrence of nighttime midlatitude spread F has been well documented in the literature considering seasonal, solar and geomagnetic variability (Bowman, 1960, Singleton, 1968; Rastogi, 1977; 1990; Huang et al., 2011). In the present study, efforts have also been made to examine the monthly occurrence of different types of spread F. It can often be observed that in the nighttime midlatitude ionosphere, various mechanisms are considered as candidates to initiate instability conditions for the formation of irregularities at the bottom of F layer which develop into certain diffused irregularity traces termed as RSF. Due to enhanced vertical plasma drift, sometimes the generated irregularities move to higher altitudes and transport these irregularities near the F layer peak. This particular type is termed as FSF. Similarly for MSF events, the irregularity density spreads all over the F region. Particularly during the annual maximum period of spread F occurrence, a unique type of spread F evolution, termed RSF-to-FSF, often characterizes the midlatitude ionosphere. Under significant vertical plasma drifts, these plasma instabilities gradually dissipate towards higher F layer altitudes which in turn generate FSF during postmidnight periods. This pattern of spread F is termed as RSF to FSF. King (1970) identified this evolution indicating that FSF is the decay product of RSF.

Figure 6a–i presents the monthly occurrence rate of different types of spread F observed over the three stations. In this figure, x axis represents the month of each year, and in primary y axis, the total number of days for each month recorded from the corresponding station is shown. In the secondary y axis, the number of observations for different types of spread F is presented, where the red column stands for FSF, green for RSF, blue for the RSF-to-FSF and yellow for MSF. Figures 7a–i 8a–i, 9a–i, 10a–i and 11a–i , illustrate the diurnal and monthly occurrence rate of overall spread F, FSF,

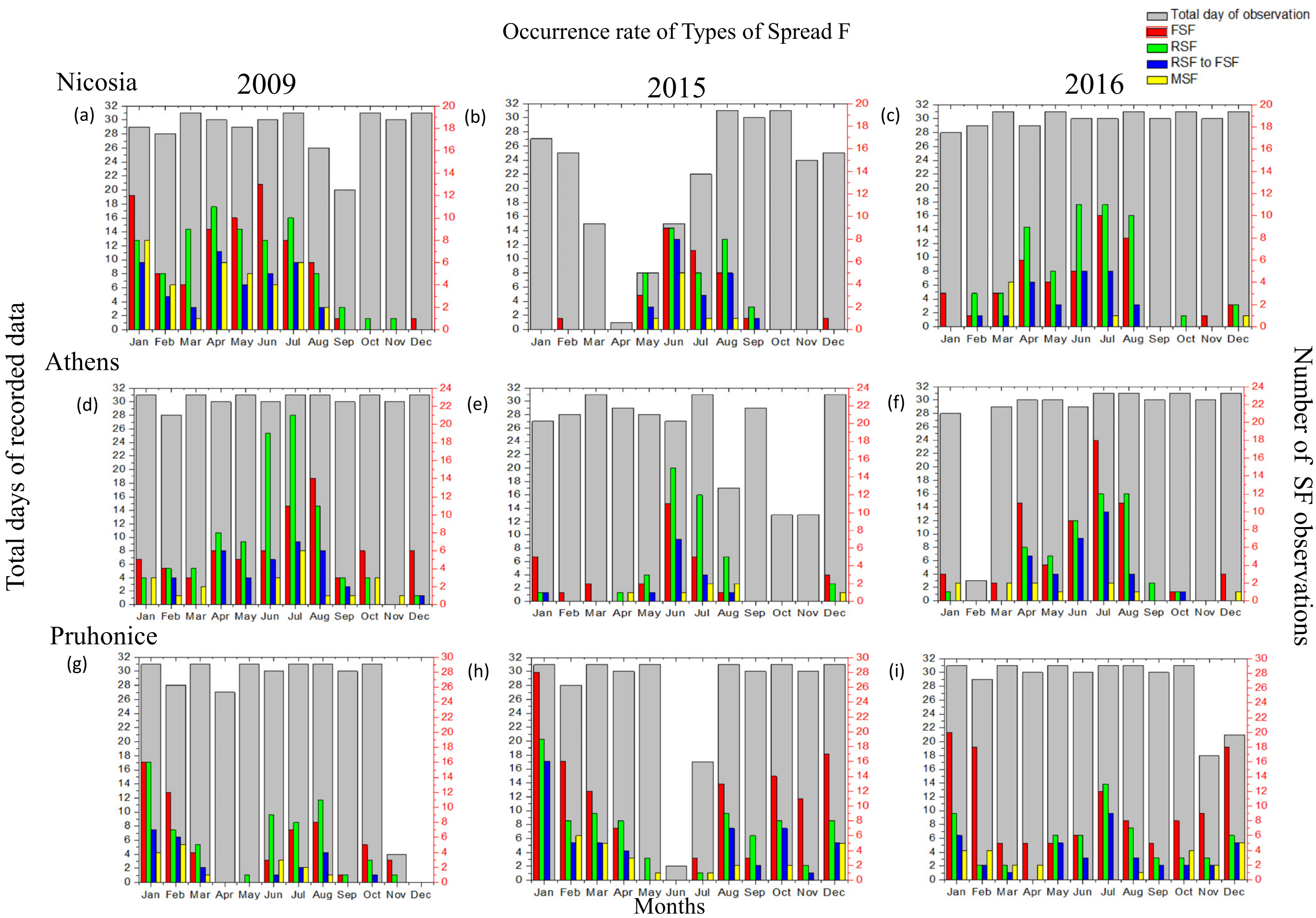

Fig. 6. Monthly variation of different spread F types observed (a) from Nicosia on 2009 (b) from Nicosia on 2015 (c) from Nicosia on 2016 (d) from Athens on 2009 (e) from Athens on 2015 (f) from Athens on 2016 (g) from Pruhonice on 2009 (h) from Pruhonice on 2015 (i) from Pruhonice on 2016.

RSF, RSF-to-FSF and MSF, respectively. In these figures, x axis shows the month of the year and the y axis shows the onset time of spread F in UT. The designated color bar represents the actual occurrence rate of spread F.

In Figure 6a, the monthly occurrence of different types of spread F over Nicosia is shown during 2009. Since 2009 was a low solar activity year, higher occurrence of spread F can be observed in summer followed by January. FSF appears more frequently around 21:00 UT to 00:00 UT during this year as shown in Figure 8a. In April, exceptionally high occurrence rate for each type of spread F is noted over Nicosia. In comparison, during fall, the number of spread F events was negligible. The monthly diurnal occurrence of spread F over Nicosia during 2009 is shown in Figure 7a. It can be observed that in April during 20:30 to 21:30 UT, maximum overall spread F occurrence (around 18 cases) were registered. Also in summer, higher rate of premidnight spread F (12–14 cases) are noted during 21:00 to 23:00 UT. In January, most of the spread F events were recorded during post sunset hours. Figures 6b and 7b present the monthly and diurnal occurrence rate of spread F types during 2015. During 2015, the reduced monthly occurrence rate for all spread F types can be attributed to high solar activity (Singleton, 1968). Spread F was recorded mostly in summer during premidnight hours (~20:00 UT to 00:00 UT) with maximum occurrence for RSF as observed in Figure 9 a–c. It is important to mention that the most frequent onset of RSF observed from Nicosia was around 21:00 UT (as shown in Figure 9a–c) during 2009 and 2016. In 2015, the RSF occurrence was limited mostly to summer. For the monthly diurnal occurrence it can be observed from Figure 7b that premidnight as well as postmidnight spread F appears during summer whereas during spring and winter, no spread F cases were recorded over Nicosia. As 2016 was a moderate solar activity year, the monthly spread F occurrence rate was higher compared to 2015 as expected. As shown in Figure 6c, the highest monthly occurrence rate for all spread F types is found in April 2016. In this year, RSF occurrence also maximized over Nicosia. From Figure 7c, it can be noted that most spread F events in summer were recorded during premidnight hours (~22:00–23:00 UT). The occurrence rate of RSF-to-FSF maximized during summer and spring around 21:00 UT to 23:00 UT at low and moderate solar activity periods as shown in Figure 10a–c. In 2015, this spread F evolution was observed during summer. Figure 11a–c present the occurrence rate of MSF over Nicosia. From these figures, it can be noted that maximum MSF occurrence was observed during winter and spring of 2009 around 20:00 UT to 23:00 UT.

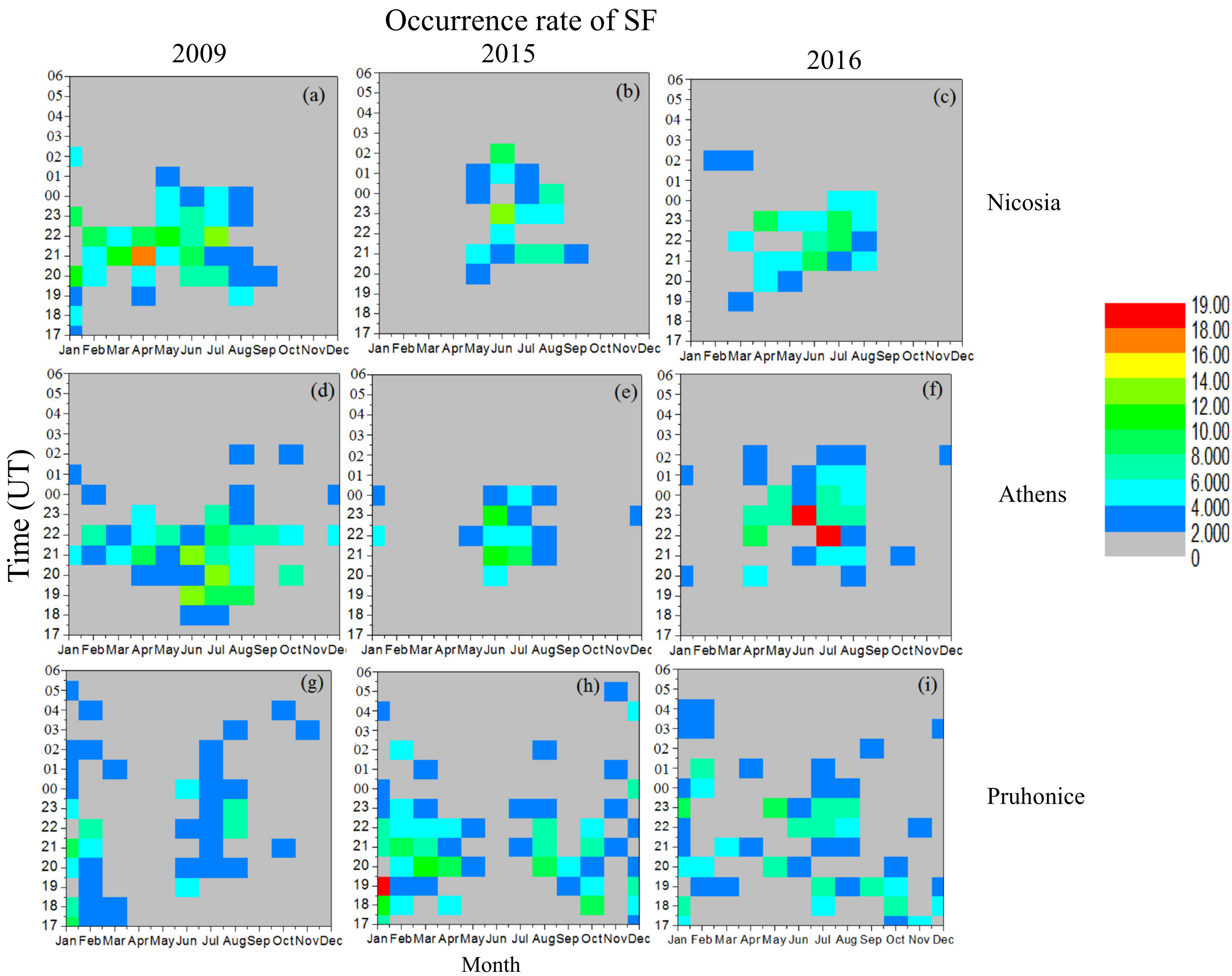

Fig. 7. Diurnal and seasonal variation of different spread F types observed (a) from Nicosia on 2009 (b) from Nicosia on 2015 (c) from Nicosia on 2016 (d) from Athens on 2009 (e) from Athens on 2015 (f) from Athens on 2016 (g) from Pruhonice on 2009 (h) from Pruhonice on 2015 (i) from Pruhonice on 2016.

Figure 6d–f represent the monthly occurrence rate of different types of spread F over Athens for 2009, 2015 and 2016, respectively and Figures 7d–f, 8d–f, 9d–f, 10d–f and 11d–f depict the corresponding monthly diurnal variation of overall spread F, FSF, RSF, RSF-to-FSF and MSF, respectively. Since the latitudinal difference between Nicosia and Athens is negligible (~2.8°), similar ionospheric behavior can be expected between the two stations. In 2009, a low solar activity year, the maximum occurrence of RSF was noted during summer around 19:00 UT to 20:00 UT, except for August. During all the equinoctial periods, a significant number of spread F cases were reported as shown in Figure 9d. During winter, spread F occurrence was lower above Nicosia station compared to summer. It can be noted from Figure 7d that during 2009 in summer, maximum number of spread F cases seems to exhibit a premidnight onset and spread F occurrence maximizes around 18:00 UT. The maximum premidnight FSF occurrence was also noted over Athens as shown in Figure 8d. Figure 9d indicates the maximum RSF occurrence during 2009 around 19:00 UT to 20:00 UT. In the equinoctial periods, spread F occurrence peaks around 22:00 UT. Figure 6e depicts monthly spread F development during 2015 (a high solar activity year) over Athens. It was observed that highest number of spread F events occurred in summer followed by winter peak. During this year no equinoctial spread F events were recorded over Athens. RSF seems to dominate during this period mostly during premidnight hours around 20:00 UT (Fig. 9e) whereas FSF was limited in June and July during the time interval 21:00 UT to 00:00 UT as shown in Figure 8e. In Figure 7e, it can be noted that a maximum number of spread F events were recorded during 21:00 to 23:00 UT for 2015 and a lower occurrence of postmidnight spread F was found during 2015. In 2016, solar activity was moderate. From Figure 6f, it is evident that the maximum number of spread F events was recorded in summer followed by spring equinox. In winter, spread F occurrence was lower compared to 2009 and 2015. Figure 7f represents the monthly diurnal variation of overall spread F occurrence. During 22:00–23:00 UT of summer solstice, maximum spread F occurrence (~19) is evident from the Figure 7f. Also spread F primarily appears from April to

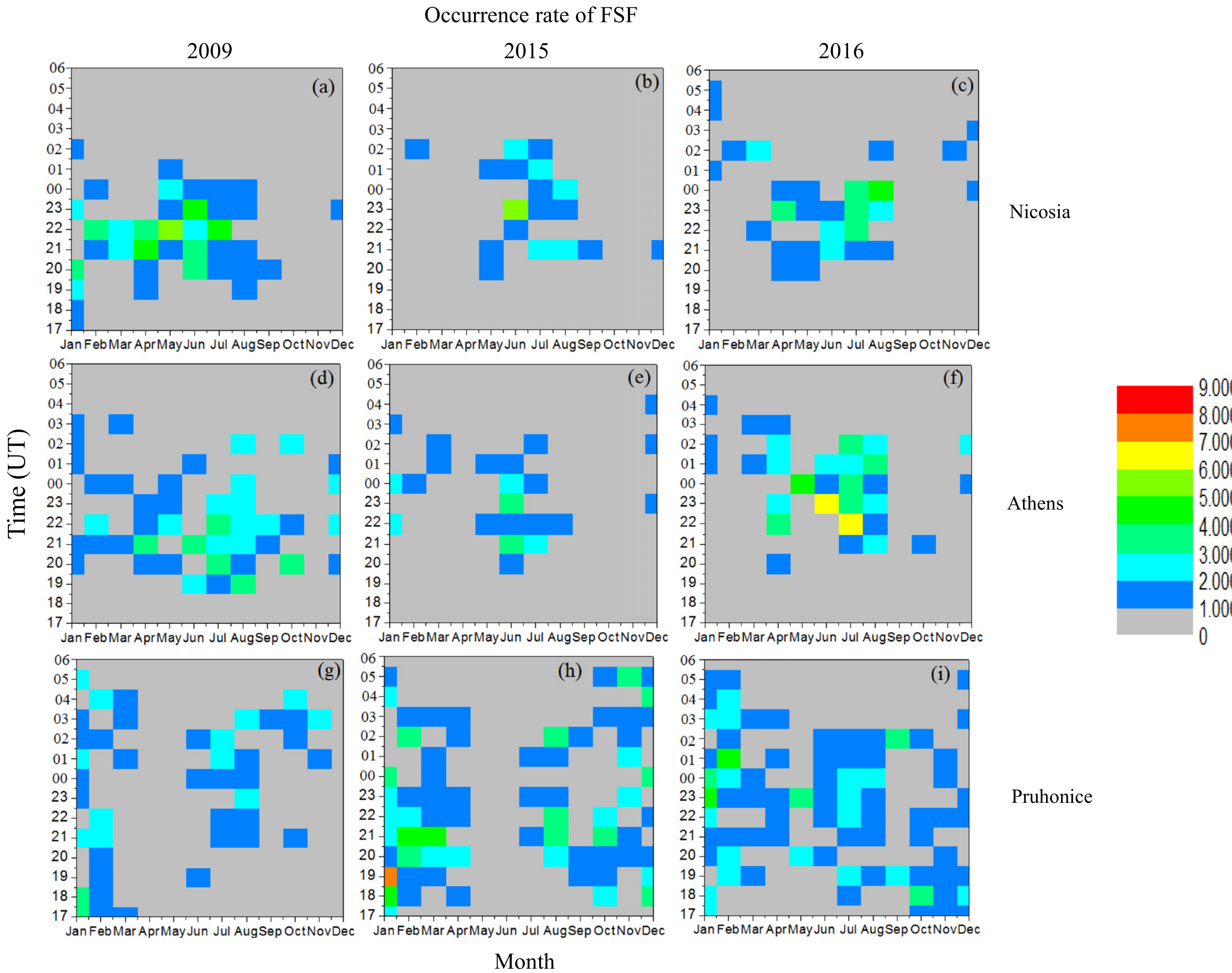

Fig. 8. Diurnal and seasonal variation of FSF observed (a) from Nicosia on 2009 (b) from Nicosia on 2015 (c) from Nicosia on 2016 (d) from Athens on 2009 (e) from Athens on 2015 (f) from Athens on 2016 (g) from Pruhonice on 2009 (h) from Pruhonice on 2015 (i) from Pruhonice on 2016.

August between 21:00 and 2:00 UT. Postmidnight spread F was observed mostly during summer. In 2016, a higher FSF occurrence rate was noted over Athens as shown in Figure 8f. Summer as well as spring was characterized by a high FSF occurrence rate during 22:00 to 2:00 UT. The occurrence rate of RSF was maximized around 22:00 UT to 23:00 UT, as shown in Figure 9f. Figure 10d–f depicts that RSF-to-FSF occurrence rate maximized around 21:00 UT to 23:00 UT for 2009, 2015 and 2016. The maximum MSF occurrence was noted in summer of 2009 between 20:00 UT and 23:00 UT. When the solar activity increased, the occurrence of MSF was reduced significantly as shown in Figure 11e–f.

Figure 6g–i present the monthly occurrence rate of spread F types and Figures 7g–i, 8g–i, 9g–i, 10g–i and 11g–i depict the monthly diurnal occurrence rate of overall spread F, FSF, RSF, RSF-to-FSF and MSF events for Pruhonice during 2009, 2015 and 2016. From Figure 6g, an annual maximum of spread F occurrence can be identified in winter, especially during January–February, and a secondary maximum appears during summer. In spite of a low solar activity, 2009 was characterized by a lower spread F occurrence. In 2009, during winter solstice the nighttime ionosphere was mostly characterized by FSF whereas in summer solstice RSF dominated. There is evidence from Figure 7g that during winter solstice, Pruhonice exhibits mostly premidnight spread F despite the fact that some spread F cases were noted just after the post-sunset periods. In summer solstice, the nighttime ionosphere exhibits both premidnight and postmidnight spread F. During 2015, maximum nighttime spread F occurrence is evident even at high solar activity. In this year, spread F was recorded during each night of January. Thus winter solstice was the primary annual maximum for 2015 dominated by FSF. During 2015, due to some technical difficulties some data gaps can be observed during summer solstice. From Figure 7h, it can be noted that most of the nighttime spread F throughout 2015 were observed before midnight. Maximum diurnal occurrence of spread F was identified during January around 19:00 UT. The monthly statistics of 2016 for Pruhonice are depicted in Figure 6i. The primary annual maximum dominated by FSF was observed during winter whereas in summer solstice RSF occurrence was significantly high. The

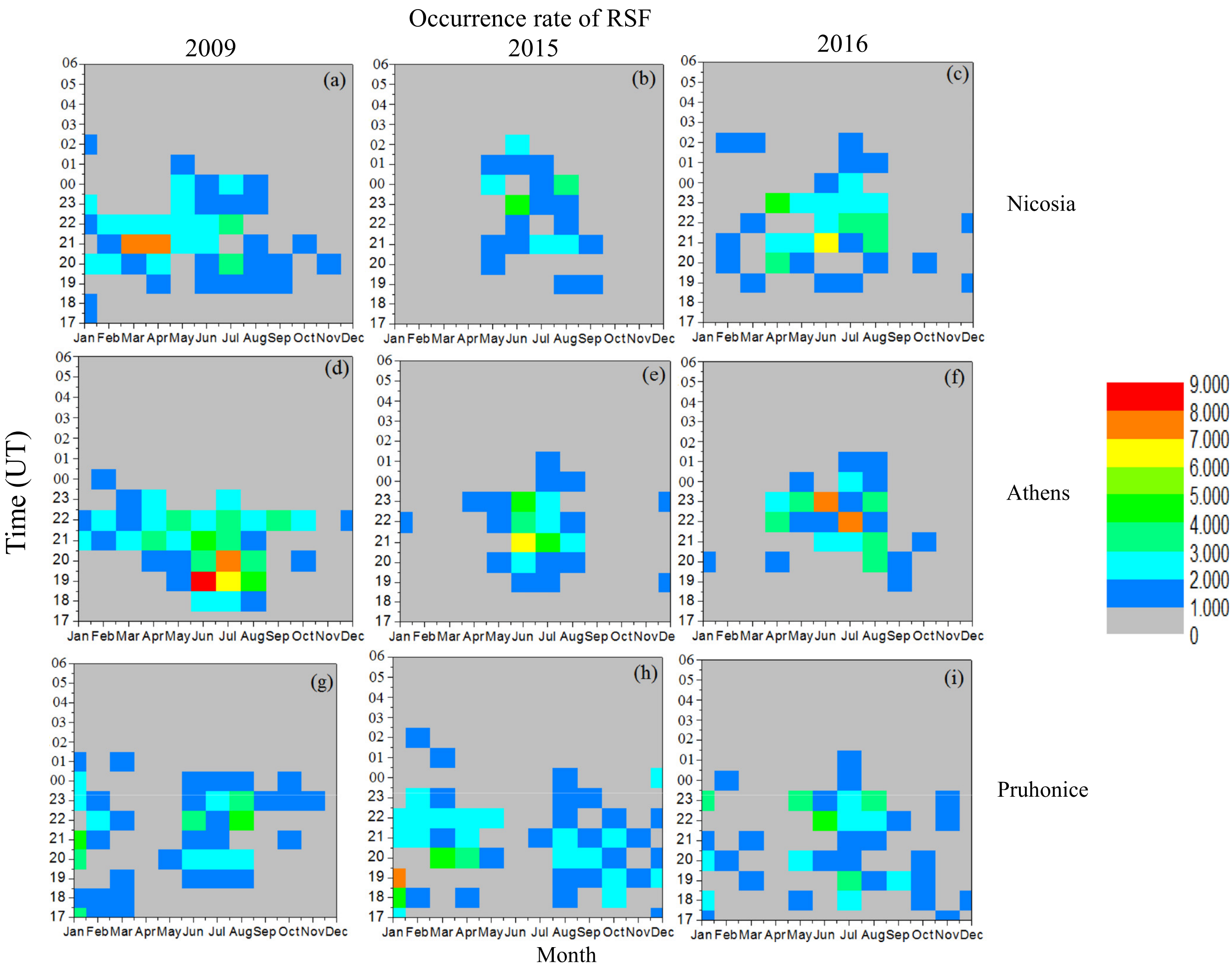

Fig. 9. Diurnal and seasonal variation of RSF observed (a) from Nicosia on 2009 (b) from Nicosia on 2015 (c) from Nicosia on 2016 (d) from Athens on 2009 (e) from Athens on 2015 (f) from Athens on 2016 (g) from Pruhonice on 2009 (h) from Pruhonice on 2015 (i) from Pruhonice on 2016.

monthly diurnal occurrence statistics is presented in Figure 7i. In this Figure, spread F onset was mostly observed during premidnight hours. Figure 8g–i depict the occurrence rate of FSF over Pruhonice. It can be observed that FSF dominated during winter. At high solar activity, FSF was frequently observed during summer and equinoxes. The RSF occurrence rate is presented in Figure 9g–i. A correlation between RSF occurrences and solar activity is clearly identified. Figure 10g–i show the occurrence rate of RSF-to-FSF. In 2015, high occurrence rate of RSF-to-FSF was recorded during winter around 18:00 UT to 19:00 UT followed by August around 20:00 UT to 21:00 UT. It can be observed from Figure 11g–i that MSF was mainly identified during January–February under low solar activity conditions (2009). Postmidnight MSF was also observed in summer during this year. When solar activity increased, the span of MSF occurrence was also extended (Fig. 11h, i) and mostly affected the premidnight ionosphere during the annual maximum of spread F occurrence in 2015 as shown in Figure 11h. In 2016, some postmidnight MSF events were also noted during January as shown in Figure 11i.

3.5 Simultaneous observations of spread F development over Nicosia, Athens and Pruhonice

Efforts have also been made to study spread F events observed simultaneously over Nicosia-Athens, Athens-Pruhonice and Nicosia-Athens-Pruhonice. Different aspects were examined corresponding to these events to identify their possible characteristics. As the longitudinal difference between Athens and Pruhonice is lower (~9°) than the latitudinal difference, in order to study the latitudinal dependence, Athens and Pruhonice were considered as a separate pair.

3.5.1 Nicosia-Athens

Figure 12a demonstrates simultaneous spread F occurrence over Nicosia and Athens. The x axis represents the year of observation, the primary y axis stands for the corresponding yearly sunspot number and the secondary y axis presents the total number of spread F observations from Nicosia (geographic Lat: 35.19 °N, Long: 33.38 °E geographic; Geomagnetic. dip: 29.38 °N) and Athens (geographic Lat: 37.98 °N, Long: 23.73 °E

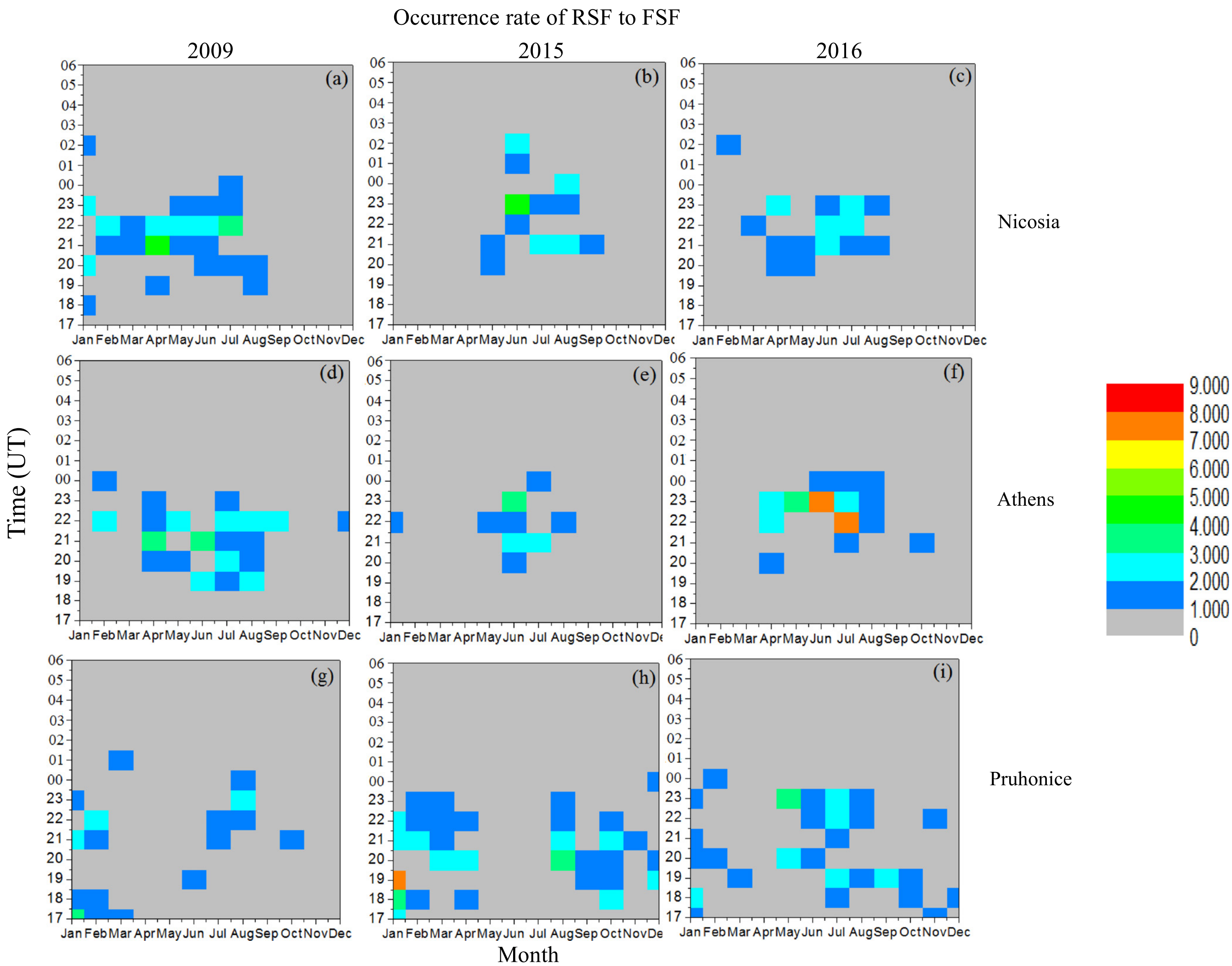

Fig. 10. Diurnal and seasonal variation of RSF-to-FSF observed (a) from Nicosia on 2009 (b) from Nicosia on 2015 (c) from Nicosia on 2016 (d) from Athens on 2009 (e) from Athens on 2015 (f) from Athens on 2016 (g) from Pruhonice on 2009 (h) from Pruhonice on 2015 (i) from Pruhonice on 2016.

geographic; Geomagnetic. dip: 34.61 °N). The column with intense tilted pattern shows the number of spread F events observed over Nicosia, the weak tilted pattern column represents spread F over Athens and the column that contains vertical lines presents the number of common spread F occurrences between Nicosia and Athens, respectively. It is important to mention that during 2009, the yearly mean value for 10.7 cm solar flux (F10.7) and sunspot number were 70.5 and 4.8, respectively which implies that the solar activity in this year was minimized. In 2009, 47 common (onset of spread F at the same time interval observed over Nicosia and Athens) were noted. In 2015 and 2016, the yearly mean values for 10.7 cm solar flux (F10.7) were 117.7 and 88.8 and yearly sunspot number were 69.8 and 39.8, respectively. 16 common spread F cases were found over these two stations in 2015 (a high solar activity year) and during 2016 (a moderate solar activity year), 37 common nighttime spread F events were observed over these two stations, respectively.

In an effort to understand the plasma dynamics of the instability mechanisms behind the common nighttime spread F events observed over the two stations with almost 10° longitude difference further analysis was performed. Figure 13a–c represent seasonal statistics of various signatures observed at ionospheric F layer as possible triggering mechanisms for spread F occurrences. The x axis represents month, primary y axis shows the number of common spread F events observed over Nicosia and Athens corresponding to each month, and the secondary y axis the number of common parameters responsible for the initiation of instability mechanism and precursors as observed over both stations prior to the onset of common spread F events. The red column represents Es occurrence and thereby signifies the electrodynamic coupling between Es and F layer prior to a spread F event, green column stands for LSWS signatures prior to spread F, blue for GPS-TID signatures, magenta for Vz-TID signature and finally yellow for F layer uplift observations. Figure 13a depicts the combined scenario of Nicosia and Athens during 2009. It can be noted that during summer, especially in June and July, maximum common spread F events were observed over these two stations. During this period almost one-to-one correspondence is noted for spread

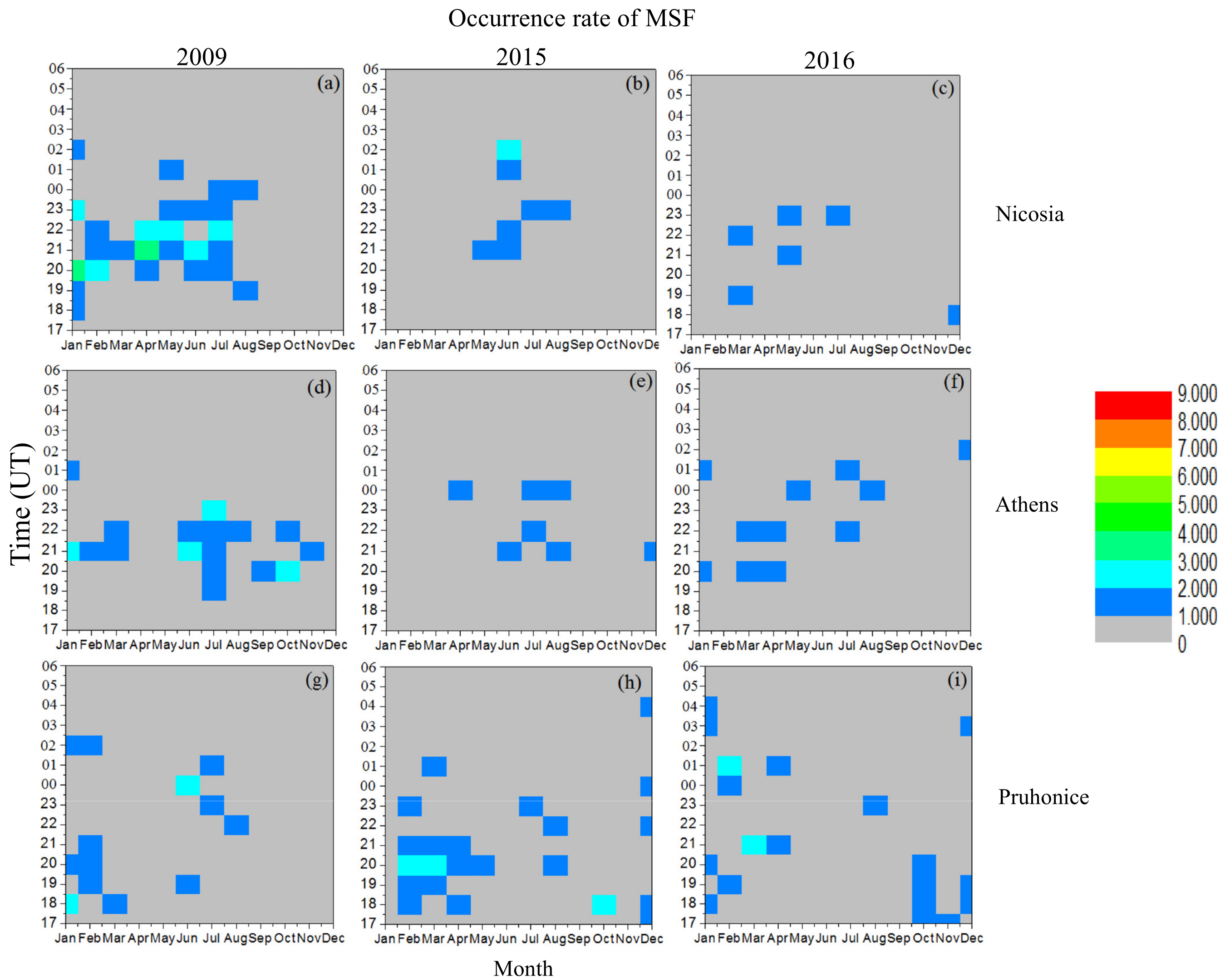

Fig. 11. Diurnal and seasonal variation of MSF observed (a) from Nicosia on 2009 (b) from Nicosia on 2015 (c) from Nicosia on 2016 (d) from Athens on 2009 (e) from Athens on 2015 (f) from Athens on 2016 (g) from Pruhonice on 2009 (h) from Pruhonice on 2015 (i) from Pruhonice on 2016.

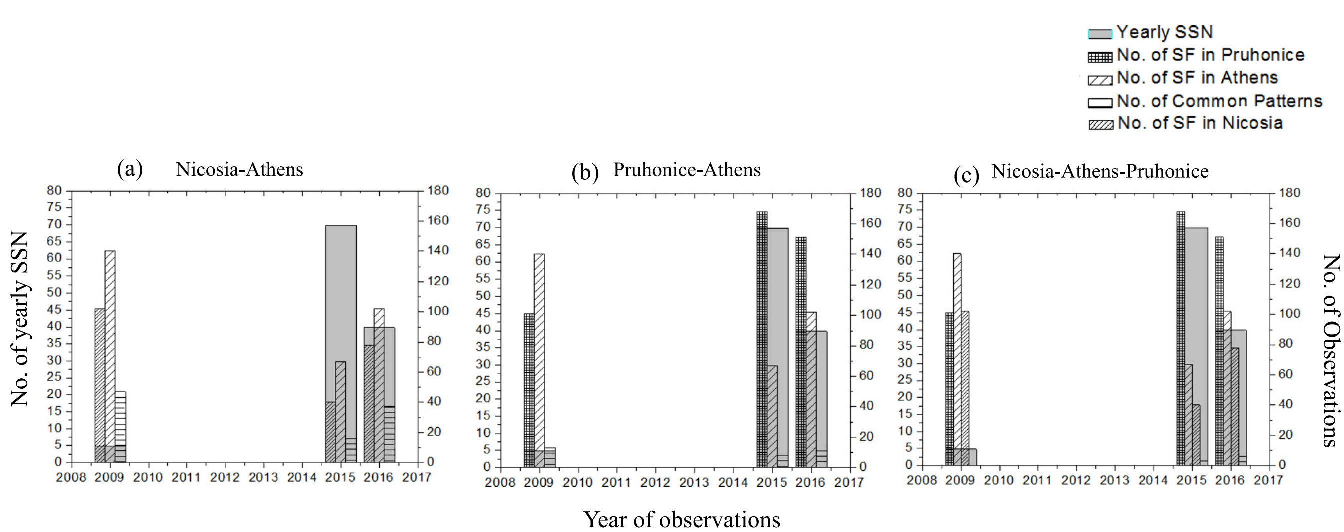

Fig. 12. Comparison of individual and common spread F observation under different solar activity from (a) Nicosia and Athens (b) Athens and Pruhonice (c) Nicosia, Athens and Pruhonice.

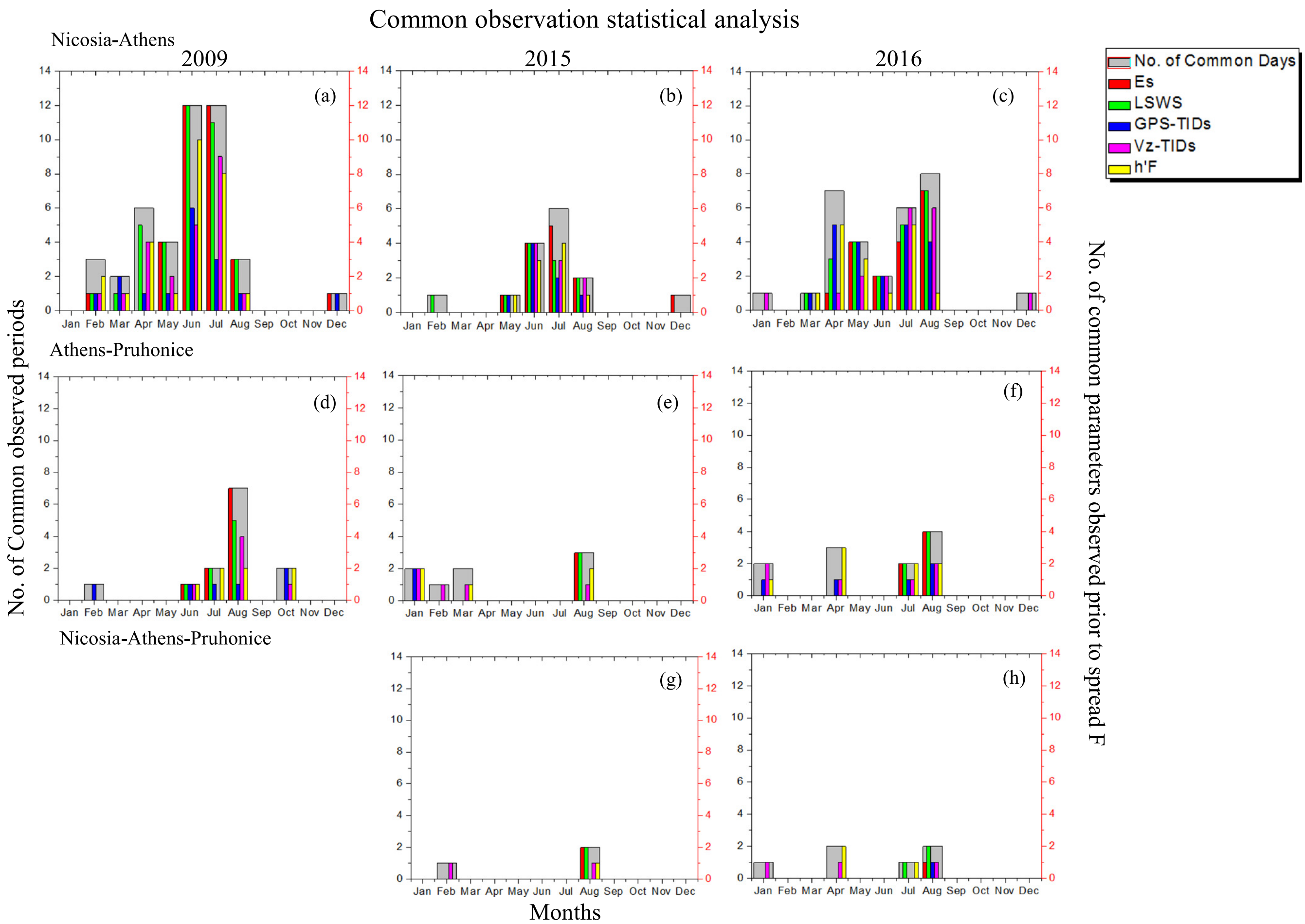

Fig. 13. Statistical analysis for different parameters and precursors observed prior to the common spread F observation from (a) Nicosia and Athens on 2009 (b) Nicosia and Athens on 2015 (c) Nicosia and Athens on 2016 (d) Athens and Pruhonice on 2009 (e) Athens and Pruhonice on 2015 (f) Athens and Pruhonice on 2016 (g) Nicosia, Athens and Pruhonice on 2015 (h) Nicosia, Athens and Pruhonice on 2016.

F events with nighttime Es layer. Also LSWS, either in the form of STs or MREs is observed as precursors prior to the onset of most of the common spread F events over Nicosia and Athens. It is important to note that during summer; almost all types of signatures were detected over both stations before the onset of spread F. During equinox, maximum occurrence of Vz-TIDs was observed prior to spread F onset over both stations. During winter, occurrence of GPS-TID signature was more prominent prior to spread F generation. In 2015, common spread F events were mostly observed during summer and similar to 2009; electrodynamic coupling between Es and F layer appeared very frequently. LSWS signatures were also quite evident during summer, and during June to August; Vz-TIDs were frequently observed prior to spread F occurrences over both stations. 2016 was a moderate solar activity year. During this year, common spread F events were observed in both summer and spring. For the summer solstice, the presence of electrodynamic coupling followed by Vz-TIDs and subsequent GPS-TIDs were noted before spread F. LSWS signatures were also frequently noted. During spring, GPS-TIDs and F layer uplifts were also observed prior to the onset of common spread F. In winter Vz-TIDs were noted before the onset of common spread F events.

3.5.2 Athens-Pruhonice

Figure 12d represents the number of common spread F events observed from Athens (geographic Lat: 37.98 °N, Long: 23.73 °E geographic; Geomagnetic. dip: 34.61 °N) and Pruhonice (geographic Lat: 50.05 °N, Long: 14.41 °E geographic; Geomagnetic. dip: 47.70 °N) during 2009 (a low solar activity year), 2015 (a high solar activity year) and 2016 (a moderate solar activity year), respectively. 13 common spread F events were noted from Athens and Pruhonice during 2009. In 2015 and 2016, the numbers of common spread F cases were 8 and 11, respectively.

Figure 13d–f depict the effects of various parameters responsible for the initiation of instability mechanism and precursors observed frequently prior to the onset of common spread F over Athens and Pruhonice. From Figure 13d–f, it is clearly observed that during low solar activity, most of the common spread F events between Athens and Pruhonice took place during summer solstice. During this time of the year, the effect of electrodynamic coupling was most evident before common spread F events followed by Vz-TIDs and F layer uplifts. LSWS as a precursor is also noted during summer. During winter solstice, significant effects of GPS-TIDs, Vz-TIDs and F layer uplifts were observed before the onset of common spread F events from Athens and Pruhonice.

3.5.3 Nicosia-Athens-Pruhonice

Figure 12c depicts the composite picture of common spread F events observed along with the individual spread F cases from the three stations, Nicosia, Athens and Pruhonice during 2009 (a low solar activity year), 2015 (a high solar activity year) and 2016 (a moderate solar activity year). In 2009, no common spread F events were found over Nicosia, Athens and Pruhonice respectively. 3 common spread F events were noted from Nicosia, Athens and Pruhonice in 2015. During 2016, 6 common spread F cases were found over the three stations.

The statistics of the contribution of different parameters responsible for the initiation of instability mechanism and precursors observed frequently prior to the onset of common spread F events from Nicosia, Athens and Pruhonice are shown in Figure 13g, h during 2015 and 2016. From Figure 13g, most of the common spread F events for 2015 were noted during summer especially in August and one-to-one correspondence was observed between the electrodynamic coupling of Es and F layer with common spread F occurrence. Vz-TIDs and F layer uplift were also noted during summer. LSWS as a precursor to spread F was also present with one-to-one correspondence in the common spread F events. During February, only Vz-TIDs were noted before the onset of common spread F events. During 2016, most of the common events were noted in the summer. LSWS showed good correspondence as a precursor to the common spread F events. For the only common spread F event observed in January, Vz-TID was present. The maximum effect of the parameters responsible for initiating instability prior to the common spread F events observed during April was F layer uplifts followed by Vz-TIDs.

4 Discussion

This paper presents the fundamental morphological aspects of nighttime spread F development considering different spread F types and spread F dependencies on solar activity, diurnal and seasonal variations over three European stations Nicosia (geographic Lat: 35.19 °N, Long: 33.38 °E geographic; Geomagnetic. dip: 29.38 °N), Athens (geographic Lat: 37.98 °N, Long: 23.73 °E geographic; Geomagnetic. dip: 34.61 °N) and Pruhonice (geographic Lat: 50.05 °N, Long: 14.41 °E geographic; Geomagnetic. dip: 47.70 °N) during 2009 (a low solar activity year), 2015 (a high solar activity year) and 2016 (a moderate solar activity year). To investigate the distinct effects of latitudinal and longitudinal variations, common spread F events were selected between Nicosia-Athens and Athens-Pruhonice stations. Different signatures and precursors, which appear prior to the triggering of instabilities in the bottom of F layer observed over both station pairs simultaneously, prior to the onset of common spread F events, and have been studied statistics have been compiled for the analyses. Several authors have studied the development and distinct features of nighttime midlatitude irregularity types (Singleton, 1968; Rastogi, 1977; Fejer & Kelley, 1980; Bowman, 1984; 1986; 1988a; 1988b; 1990; Haldoupis et al., 2003; Huang et al., 2011). *Perkins* and *gradient drift instabilities* are considered to be the most probable mechanisms for the generation of nighttime midlatitude irregularities. But only these irregularity mechanisms are not sufficient to support spread F development in accordance with the observations. The background neutral density of the nighttime ionosphere also affects the generation mechanism of spread F events. Kotake et al. (2006) showed a semiannual variation of neutral density with solar activity. Hines (1960) suggested an inverse correlation between gravity wave activity and neutral density distribution over midlatitude ionosphere. *Perkins instability* (Perkins, 1973) also involves an inverse association with neutral density. These factors indicate that for high neutral densities, lower rate of plasma density perturbation would take place in the F layer, which in turn reduces the probability of TID generation and also affects significantly the development of spread F events (Kelley & Fukao, 1991). To analyze the observations, various signatures have been identified in the literature which may initiate the instability mechanisms, as well as accelerate the irregularity generation process. Among those, the major mechanisms that mostly affect the nighttime ionosphere over the midlatitude region are: (1) the electrodynamic coupling between Es and F layer which significantly affects the Es layer perturbation and creates a large positive feedback polarization electric field, mapping with a direction of NW to SE from the E layer to bottom of F layer. This in turn amplifies the instability perturbation and accelerates irregularity generation (Haldoupis et al., 2003; Cosgrove & Tsunoda, 2004; Cosgrove, 2007). (2) gravity waves also play a dominant role as a driving mechanism. It can be observed that a wave driven density perturbation affects the bottom of the F region and causes initiation of the instability mechanism. Subsequently, the irregularities generated from instability mechanisms overlap with large scale horizontal and vertical density gradients that develop from gravity waves in the background ionosphere and give rise to spread F (Bowman, 1990, 1991). (3) Swartz et al. (2002) suggested F layer uplifts (h′F) associated with TIDs that can also drive the instability mechanism at the bottom of the F layer and may lead to irregularity generation and spread F.

The diurnal variation of the nighttime spread F occurrence has been investigated in detail over the three stations. As discussed in Figure 4a–c, the diurnal variation of nighttime spread F observed over Nicosia and Athens during 2009, 2015 and 2016 clearly shows a similar trend which may imply that for these two low midlatitude stations, the variation of nighttime ionosphere is significantly correlated. On the other hand Pruhonice is situated at higher latitude (50.05 °N). A distinct difference can be noted in the diurnal spread F variations observed over Pruhonice mostly in winter, especially in the months of January and February. Bowman (1960) studied the diurnal variability of different types of spread F from Brisbane and Townsville (Lat: 19.6 °S, Long: 146.8 °E geographic: geomagnetic Lat: 41.36 °N) and identified a peak of RSF occurrence around midnight, which is also depicted in the present study. In case of FSF events, a peak just before sunrise was identified by Bowman (1960) which supports the results of FSF diurnal variability shown in the present paper. Bhaneja et al. (2009) studied the seasonal and solar cycle variation of midlatitude spread F from Wallops

Island (Lat: 37.95 °N, Long: 284.53 °E geographic: geomagnetic dip: 67.5°) and have recorded long duration spread F events during winter of low solar activity periods. Singleton (1968) reported the annual maximum of spread F occurrence during winter around the geographic latitude of 50 °N. During winter, in the higher midlatitude ionosphere, early sunset can be noted which in turn introduces a sudden downward excursion of vertical plasma drift of F layer, and initiates the instability mechanism at the convergence of Es and F layers. During post sunset hours, in the presence of NW to SE coupled electric dynamo and Earth's magnetic field, a horizontal movement of plasma density has often been observed which eventually uplifts the irregularity distributions to higher altitudes and FSF develops. In the postmidnight periods, the decay rate of these nighttime irregularities are reduced due to high alignment between magnetic field lines of nighttime F layer with the sunset terminator which in turn elongates the diurnal extent of nighttime spread F observed in the higher midlatitude regions. Upadhayaya & Gupta (2014) observed spread F events with extended duration (~18:00-08:00 LT) in high solar activity period from the Indian longitude sector. The occurrence of nighttime spread F exhibits clear solar cycle dependence (Bowman, 1960; Singleton, 1968; 1998, 2001; Wang et al., 2010). Bowman (1998) related sunspot number with nighttime midlatitude spread F occurrence rate. It can be observed from Figure 5a, b that spread F occurrence clearly shows an inverse correlation with sunspot number which is well established in the literature (Singleton, 1968; Bowman, 1998; Bhaneja et al., 2009). But from Figure 5c, positive correlation between the occurrence of nighttime spread F and sunspot number was noted from Pruhonice. These results clearly show that solar activity affects the occurrence of nighttime spread F at higher midlatitudes. Singleton (1957) suggested this inverse solar activity dependence over the probability of spread F occurrence rate at higher midlatitudes to originate from auroral activity. Also during high solar activity, the occurrence rate of FSF maximized compared to RSF over Pruhonice. Singleton (1968) reported a higher occurrence of spread F at higher midlatitude regions (around 50°N) during high solar activity compared to low solar activity periods. According to that study, the temporal variation of FSF occurrence advances with geomagnetic latitude in a way equivalent to high solar activity. During high solar activity, the nighttime irregularity generation at lower midlatitudes reduces significantly due to the presence of high upper atmosphere neutral particle density, which in turn imposes a negative influence over the wave amplitude of TIDs and reduces the triggering effect for nighttime irregularity generation (Bowman, 1960). Chapagain et al. (2009) performed radar observations from 1996 to 2006 over post sunset equatorial spread F irregularities from Jicamarca (Lat: 12 °S, Long: 283.2 °E geographic: geomagnetic Lat: 1.14 °N). They observed that the average onset height of spread F events intensified significantly with solar activity but the onset time of spread F events showed no dependence over solar flux. It can be suggested that during higher solar activity periods, the generation of midlatitude irregularities reduces significantly. The disturbances initiated by auroral activity and created in the polar region due to Auroral Electrojets (AEs) may affect subauroral regions and initiate large scale TIDs which may propagate equatorward during post sunset hours (Hajkowicz, 2016 and the references therein).

The seasonal variability of nighttime midlatitude spread F has been reported by several authors (Singleton, 1968; Bowman, 1998; Bhaneja et al., 2009; Deminov et al., 2009; Amabayo et al., 2011). Singleton (1968) suggested that FSF occurrence maximizes around 40° to 50° in latitude, whereas RSF dominates between 45° to 55°. Chen et al. (2011) observed that the rate of nighttime spread F maximized over the Chinese midlatitude sector during summer. Similarly, by using ionosonde measurements around American, Pacific and Southeast Asian latitudinal regions, Li et al. (2011) noted that the occurrence rate of midlatitude spread F maximized during midnight to postmidnight hours during June solstice, especially at solar minimum. However, they did not observe any GPS TEC fast fluctuations, which verified the absence of GPS scintillations in the postmidnight ionosphere during low solar activity periods. Zhang et al. (2015) studied the effect of postmidnight spread F in terms of Quasi Frequency (QF) and GPS scintillations from Sanya (Lat: 18.34 °N, Long: 109.42 °E geographic: geomagnetic Lat: 22.67 °N), and suggested that in the equinoctial periods, the postmidnight ionosphere would equally be affected by QF and GPS scintillations due to the presence of both small scale (~400 m) and large scale (~several kilometers) irregularities. But during June solstice, the postmidnight ionosphere is mainly affected by TIDs and Es activity, which in turn maximizes the probability of spread F occurrence. Lambert (1988) studied the disturbance pattern of midlatitude ionospheric F layer from Johannesburg (Lat: 24.04 °S, Long: 28.06 °E geographic: geomagnetic Lat: 47.72 °S) and Hermanus (Lat: 34.25 °S, Long: 19.13 °E geographic: geomagnetic Lat: 51.03 °S). It was observed that the disturbance probability in the nighttime midlatitude ionosphere minimized during autumn (8%) which is in agreement with the results reported in this paper. The annual maxima of spread F during winter was identified followed by secondary maxima during summer. Amabayo et al. (2011) also analyzed spread F occurrence over Grahamstown (Lat: 33.32 °S, Long: 26.5 °E geographic: geomagnetic Lat: 50.41 °S) and Madimbo (Lat: 22.38 °S, Long: 30.88 °E geographic: geomagnetic Lat: 46.67 °S) and reported that the diurnal occurrence of spread F increases mostly around 23:00–24:00 UT and the seasonal peak of spread F occurrence around winter. It can be noted that over both Nicosia and Athens, the occurrence rate of nighttime spread F maximized during the summer irrespective of solar activity followed by a secondary maximum either at winter or at spring which may signify solar cycle dependence. During 2009, over Nicosia and Athens, FSF dominated, which may indicate the presence of strong coupled electric field and horizontal plasma drift velocity shearing mechanism to explain transport of nighttime irregularities to higher F layer altitude which evolved into FSF. In 2015 and 2016, during high and moderate solar activity, RSF dominated. Surprisingly in the case of Athens, the effects of frequency spreading dominated with range spreading in 2016 whereas in 2009 and 2015, the nighttime ionosphere was mostly affected by RSF events. These statistics suggest that types of spread F observed may depend on the instability induced by unstable Es layers, which eventually couple to the bottom of F layer and play a decisive driving role to initiate large scale irregularity distributions as well as boost the coupled NW to SE electric field structures. This in turn control spread F development (Herman, 1966; Yokoyama et al., 2009).

Table 2. Percentage observations of different signatures prior to the common spread F occurrence.

Year	Station combinations used	Unstable Es (%)	LSWS (%)	GPS-TIDs (%)	Vz-TIDs (%)	F layer uplift (%)
2009	Nicosia-Athens	76.74	86.05	34.88	53.49	62.79
	Athens-Pruhonice	76.92	61.54	46.15	46.15	53.85
	Nicosia-Athens-Pruhonice	–	–	–	–	–
2015	Nicosia-Athens	86.67	73.33	53.33	53.33	53.33
	Athens-Pruhonice	37.50	37.50	25.00	62.50	62.50
	Nicosia-Athens-Pruhonice	66.67	66.67	0.00	66.67	33.33
2016	Nicosia-Athens	58.06	70.97	67.74	61.29	54.84
	Athens-Pruhonice	54.55	54.55	45.45	54.55	72.73
	Nicosia-Athens-Pruhonice	16.67	50.00	16.67	50.00	50.00

Deminov et al. (2009 and the references therein) have noted the probability of occurrence of nighttime spread F over higher midlatitude ionosphere of the European longitude sector and found that during winter solstice spread F occurrence maximizes followed by a semiannual summer maximum (Singleton, 1968). In the present paper, the occurrence of nighttime spread F has been studied for high midlatitude station Pruhonice (geographic Lat: 50.05 °N, Long: 14.41 °E geographic; Geomagnetic. dip: 47.70 °N) also. The present analysis shows that the annual maxima for nighttime spread F occurrence over Pruhonice is normally observed during winter irrespective of solar activity, as observed by Singleton (1968). Secondary maxima of nighttime spread F occurrence may exhibit solar cycle dependence and is observed during summer solstices during low and moderate solar activity and during spring at high solar activity. At annual maxima of nighttime spread F, FSF dominates over Pruhonice, whereas during secondary maxima, RSF was noted to be prominent. These statistics suggest that during winter, the irregularity distributions mainly affect the higher altitudes of F layer. Bhaneja et al. (2009) observed that during maximum solar activity, the effect of frequency spreading is more frequent possibly due to auroral activity, which implies that the irregularity distributions may flow from polar to the sub auroral regions when the effects of driving mechanisms in the nighttime midlatitude ionosphere diminish. However these findings require further investigation, which may indicate the interaction between higher midlatitude and auroral irregularity distributions under quiet magnetic conditions. After the post sunset period, the instability mechanisms are initiated at the bottom of the F layer and generate irregularities that develop into range spread F. Gradually during postmidnight hours, in the presence of upward plasma drift, these irregularities may drift from the F layer bottom to higher altitudes. Thus the trace of RSF may evolve into FSF mostly observed during postmidnight periods as shown in Figure 10a–i. It can be seen from this figure that this type of spread F is only observed when the duration of spread F lasts up to postmidnight hours and mostly during the annual maxima period of spread F.

The longitudinal and latitudinal dependence of spread F generation has been well studied in the literature (Shimazaki, 1962; Singleton, 1968; Rastogi, 1977; Mwene et al., 2004; Hajkowicz, 2007; Bhaneja et al., 2009; Huang et al., 2011). Singleton (1968) investigated the seasonal variability of spread F with solar activity over a wide latitudinal extent. He observed three main regions with high irregularity occurrences, namely, equatorial region up to 40°, high latitudinal region (≥70°) and higher midlatitude region (>50°). Hajkowicz (2007) observed a global pattern of enhanced spread F activity during June solstice from the Japanese longitude sector.

Gravity waves are considered one of the important driving mechanisms for midlatitude spread F. Since gravity waves originate primarily in the lower atmosphere, different meteorological conditions have been clearly observed over gravity wave formation. Huang et al. (2011) observed significant difference in spread F occurrence between Changchun (Lat: 43.8 °N, Long: 125.26 °E geographic: geomagnetic Lat: 36.76 °N) and Urumqi (Lat: 43.75 °N, Long: 87.63 °E geographic: geomagnetic Lat: 33.08 °N) stations in China which have 38° longitudinal separation. In the present paper, to study the effect of longitudinal dependency over spread F generation, common spread F events at the same time period during the same day of the year observed over Nicosia and Athens were considered for 2009, 2015 and 2016. Nicosia and Athens are situated with 10° longitude separation (Tab. 1). It can be observed in Figure 13a–c that the electrodynamic coupling between Es and the bottom of F layer, acting to initiate the instability mechanism responsible for spread F development, is significant. LSWS signatures were noted as precursors to these common spread F events observed over both Nicosia (geographic Lat: 35.19 °N, Long: 33.38 °E geographic; Geomagnetic. dip: 29.38 °N) and Athens (geographic Lat: 37.98 °N, Long: 23.73 °E geographic; Geomagnetic. dip: 34.61 °N). Table 2 presents an overview for various signatures observed prior to the onset of common spread F events. It can be concluded that during 2009 and 2015, the main mechanisms were the electrodynamic coupling between Es and F layer followed by F layer uplifts which may be influenced by wave amplitude patterns normally observed in the nighttime midlatitude ionosphere (Hines, 1963). Harman (1966 and the references therein) suggested that the peak occurrence of spread F during evening hours may have a direct correlation with F layer uplift and a large amplitude shift in F layer uplift ($\Delta h'F_{max}$) may take place. Also spread F development may exhibit a certain time lag with respect to maximum F layer uplift. Bowman (2001) observed the dependence of F_2 layer height on the presence of TIDs in the midlatitude nighttime ionosphere from different latitude regions and concluded that F layer uplifts associated with spread F development and TIDs can be found from the equator to auroral region as a driving mechanism for instability generation in the nighttime ionosphere. To investigate the effect of nighttime TIDs over spread F occurrence, Shiokawa et al. (2003) studied the statistical features of nighttime TIDs using 630-nm airglow images from two midlatitude stations in the Japanese longitude sector during 1998–2000. They observed that the occurrence rate for both TIDs and spread F events were quite similar and had a major peak during summer solstice followed by a minor peak in winter. Lee & Chen (2015) and Bowman (2001) also observed a similar behavior of nighttime TID patterns from Chung-Li (Lat: 24.97 °N, Long: 121.2 °E geographic: geomagnetic Lat: 33.14 °N). It has been suggested (Otsuka et al., 2009) that the secondary peak of TID activity observed in winter could be attributed to the higher probability of Es development during summer over Australian longitudes. Southeastward and equator ward propagation has also been noted for nighttime TID events (Behnke, 1979; Evans et al., 1983; Shiokawa et al., 2003) for all seasons which may not be described in terms of gravity waves. The *Perkins instability* mechanism may control this direction of propagation (Shiokawa et al., 2003) of nighttime TID patterns. Almost one-to-one correspondence was found between the spread F occurrences with LSWS, as a precursor. In 2016, Vz-TID and GPS-TID activity dominate over the nighttime ionosphere of Nicosia and Athens before the onset of common spread F events. Kotake et al. (2006) observed a major peak of nighttime TID activity for European longitude sector during summer whereas the maximum spread F occurrence was noted in winter. Opposite scenario was observed in the American longitude sector. Thus the authors demonstrated the latitudinal variation of nighttime TID events and suggested that the difference between TID activity and spread F occurrence was observed due to the variability of spatial scale sizes of irregularity distributions detected by GPS TEC and the source of spread F events. To observe nighttime TID activities, Chen et al. (2011) studied the amplitude fluctuations with respect to background TEC exceeding 1% from Sanya. Ding et al. (2011) also found similar nighttime TID patterns at Wuhan station (Lat: 30.5 °N, Long: 114.4 °E geographic: geomagnetic Lat: 20 °N), which is situated along the same longitude as Sanya station. LSWS occurrence reduced in 2016 for common spread F events. To study the latitudinal dependence of nighttime midlatitude spread F occurrence, ionograms from Athens and Pruhonice have been used. From Table 1, it can be noted that these two stations have 13° latitudinal separation whereas longitudinally the separation is around 9°. It can be observed that during low solar activity conditions, the electrodynamic coupling between Es and F layers serves as the main instability mechanism, whereas during high solar activity periods, the effect of Vz-TIDs and F layer uplift dominates the nighttime ionosphere prior to the onset of common spread F events. During 2016, significant F layer uplift was noted prior to the onset of common spread F events observed over Athens and Pruhonice. Surprisingly, LSWS was not dominant for these spread F events. The annual maximum was observed at Pruhonice in winter contrary to Athens, where it is during summer. For Pruhonice, spread F occurrence has a direct correlation with solar activity whereas for Athens an inverse correlation exists. On the other hand, almost similar characteristics have been noted between Nicosia and Athens. Common spread F events observed over Nicosia, Athens and Pruhonice were also considered. From Table 2, the effects of electrodynamic coupled electric fields between Es and F layer, Vz-TIDs and the F layer uplifts have been noted prior to common spread F events. Overall, it can be concluded that the nighttime ionosphere of the higher midlatitude European sector has different characteristics than the lower midlatitude region. Further studies are required to clarify such differences observed in the spread F occurrence rate and the impact of mechanisms responsible for initiating instabilities over different midlatitude sectors.

5 Conclusion

The present study deals with the occurrence rate of nighttime spread F events and their diurnal, seasonal and solar cycle variations observed from three stations in the European longitude sectors (Nicosia, Athens and Pruhonice) during 2009, 2015 and 2016. The latitudinal and longitudinal variation of spread F occurrence was examined by considering different instability triggering mechanisms and precursors. The main findings are summarized as follows:

- the occurrence of spread F with extended diurnal period was obtained during winter at all three stations involved in the analyses. It may be suggested that due to a close alignment between sunset terminator with the local magnetic field lines, the decay rate of postmidnight irregularity distributions may reduce significantly in the F layer which in turn may allow diffused pattern of plasma density to persist in the F region for extended periods;
- a clear inverse correlation was observed between the occurrence rate of spread F events with solar activity at lower midlatitude regions (<50 °N), as is well established in literature (Singleton, 1968; Bowman, 1998; 2001; Bhaneja et al., 2009). But at higher midlatitude regions (>50 °N), the exact opposite phenomenon is noted. In Pruhonice (situated beyond 50 °N) the occurrence rate of spread F events increases with solar activity (Singleton, 1968);
- the annual maxima of spread F occurrence over the lower midlatitude region (<50 °N) are found during summer solstices and are independent of solar activity (Huang et al., 2011) followed by a secondary maximum, which depends on solar activity. During high solar activity, no secondary maxima were detected, whereas during solar minimum, the secondary maximum was observed during winter. At moderate solar activity, it shifted to spring;
- at higher midlatitude regions (>50 °N), the annual maximum of spread F was noted in winter irrespective of solar activity whereas secondary maxima were observed during summer solstices at low and moderate solar activity, and shifted to spring during high solar activity;
- during high solar activity, nighttime F region of the lower midlatitude regions is mostly affected by RSF events, whereas FSF plays the dominant role at higher midlatitudes (Singleton, 1968; Bhaneja et al., 2009);
- longitudinal variation in spread F events observed between Nicosia and Athens was insignificant. Most probably the main instability triggering mechanisms were the electrodynamic coupling effect between Es and the bottom of F

layer, and the F layer uplift (h′F). LSWS signatures were notably observed from both these regions;

– latitudinal differences in spread F events were very prominent between Athens and Pruhonice (Singleton, 1968). The main instability triggering mechanisms were Vz-TIDs and F layer uplifts (h′F). Prominent impact of the electrodynamic coupling between Es and F layer was also noted during low solar activity to initiate the instability at higher midlatitudes.

Acknowledgements. This work has been supported by Erasmus Mundus LEADERS project for Ph.D mobility program in the form of support to visit Frederick University, Cyprus for one of the coauthors as Doctoral fellow. Authors are thankful to Dr. Chris Meek, Institute of Space and Atmospheric studies, University of Saskatchewan, Canada for providing the code for HTI plots. Contribution of Dalia Buresova is supported by the Czech Science Foundation via Grant 15-07281J. The authors would also like to thank World Data Centre (Kyoto) for providing the geomagnetic data which was very helpful for the present paper (website: http://wdc.kugi.kyoto-u.ac.jp/wdc/Sec3.html). The drift velocity data downloaded from Nicosia, Athens and Pruhonice has been analyzed with the help of Drift Explorer (http://giro.uml.edu/drift-explorer.html). Authors are also thankful to GIRO (Digital Drift DataBase) web portal (http://ulcar.uml.edu/DIDBase/). The 15 min snapshot for overall TEC distribution over the European longitude sector used in the present study has been obtained from http://www.bath.ac.uk/elec-eng/invert/iono/rti.html. The editor thanks Bruno Zolesi and an anonymous referee for their assistance in evaluating this paper.

References

Abdu MA, Batista IS, Bittencourt JA. 1981. Some characteristics of spread F at the magnetic equatorial station Fortaleza. *J Geophys Res* **86**: 6836–6842.

Abdu MA, Batista IS, Sobral JHA. 1992. A new aspect of magnetic declination control of equatorial spread F and F region dynamo. *J Geophys Res* **97**: 14897–14904.

Amabayo EB, McKinnel LA, Cilliers PJ. 2011. Statistical characterization of spread F over South Africa. *Adv Spec Res* **48**: 2043–2052.

Basu S, Basu S. 1976. Correlated measurements of scintillations and in situ F region irregularities from OGO-6. *Geophys Res Lett* **3**: 681–684.

Basu S, Whitney HE. 1983. The temporal structure of intensity scintillations near the magnetic equator. *Radio Sci* **18**: 263–271.

Basu S, Basu S. 1985. Equatorial scintillations: advances since ISEA-6. *J Atmos Terr Phys* **47**: 753–768.

Batista IS, Abdu MA, Bittencourt JA. 1986. Equatorial F region vertical plasma drifts: seasonal and longitudinal asymmetries in the American sector. *J Geophys Res* **91**: 12055–12064.

Behnke R. 1979. F layer height bands in the nocturnal ionosphere over Arecibo. *J Geophys Res* **84**: 974–978.

Beran L, Chmelar P, Rejfek L, Chum J, Mosna Z. 2015. Comparison of devices for monitoring of the ionosphere at the observatory Pruhonice. Microwave Techniques (COMITE), 2015 Conference on IEEE, pp. 1–4.

Bhaneja P, Earle GD, Bishop RL, Bullett TW, Mabie J, Redmon R. 2009. A statistical study of midlatitude spread F at Wallops Island, Virginia. *J Geophys Res* **114**: A04301. DOI:10.1029/2008JA013212.

Booker HG, Wells HW. 1938. Scattering of radio waves by the F-region of the ionosphere. *Terr Magn Atmos Electr* **43**: 249–256.

Bowman GG. 1960. Further studies of Spread-F at Brisbane-I experimental. *Planet Space Sci* :**2** 133–149.

Bowman GG. 1984. A comparison of mid-latitude and equatorial-latitude spread-F characteristics. *J Atmos Terr Phys* **46**: 65–71.

Bowman GG. 1986. Some F2 layer-sporadic-E relationships. *Ann Geophys* **4**: 55–60.

Bowman GG. 1988a. Large-scale ionospheric structures associated with mid-latitude spread F. *J Geophys Res* **93**: 5955–5958.

Bowman GG. 1988b. Small-scale stratifications associated with daytime travelling ionospheric disturbances in mid-latitude regions. *Ann Geophys* **6**: 187–194.

Bowman GG. 1990. A review of some recent work on mid-latitude spread-F occurrence as detected by Ionosondes. *J Geomagn Geoelectr* **42**: 109–138.

Bowman GG. 1991. Ionospheric frequency spread and its relationship with range spread in mid-latitude regions. *J Geophys Res* **96**: 9745–9753.

Bowman GG. 1998. Short-term delays (hours) of ionospheric spread F occurrence at a range of latitudes, following geomagnetic activity. *J Geophys Res* **103**: 11627–11634.

Bowman GG. 2001. A comparison of nighttime TID characteristics between equatorial-ionospheric-anomaly crest and midlatitude regions, related to spread F occurrence. *J Geophys Res* **106**: 1761–1769.

Chandra H, Sharma S, Abdu MA, Batista IS. 2003. SpreadF at anomaly crest regions in the Indian and American longitudes. *Adv Space Res* **31**: 717–727. DOI:10.1016/S0273-1177(03)00034-6.

Chapagain NP, Fejer BG, Chau JL. 2009. Climatology of postsunset equatorial spread F over Jicamarca. *J Geophys Res* **114**. DOI:10.1029/2008JA013911.

Chen WS, Lee CC, Chu FD, Su SY. 2011. Spread F, GPS phase fluctuations, and medium-scale traveling ionospheric disturbances over Wuhan during solar maximum. *J Atmos Sol Terr Phys* **73**: 528–533.

Cosgrove RB. 2007. Generation of mesoscale F layer structure and electric fields by the combined Perkins and E s layer instabilities, in simulations. *Ann Geophys* **25**: 1579–1601.

Cosgrove RB, Tsunoda RT. 2004. Instability of the E-F coupled nighttime midlatitude ionosphere. *J Geophys Res* **109**: A04305. DOI: 10.1029/2003JA010243.

Deminov MG, Deminov RG, Nepomnyashchaya EV. 2009. Seasonal features in the spread-F probability near midnight over Moscow. *Geomagn Aeron* **49**: 630–636.

Ding F, Wan W, Xu G, Yu T, Yang G, Wang J. 2011. Climatology of medium-scale traveling ionospheric disturbances observed by a GPS network in central China. *J Geophys Res* **116**: 19. DOI: 10.1029/2011JA016545.

Earle GD, Musumba AM, McClure JP. 2006. A global study of nighttime midlatitude topside spread echoes. *J Geophys Res* **111**: A11306. DOI:10.1029/2006JA011614.

Earle GD, Musumba AM, Vadas SL. 2008. Satellite-based measurements of gravity wave-induced midlatitude plasma density perturbations. *J Geophys Res* **113**: 6 DOI:10.1029/2007JA012766.

Earle GD, Bhaneja P, Roddy PA, Swenson CM, Barjatya A, Bishop RL, Bullett TW, Crowley G, Redmon R, Groves K, Cosgrove R. 2010. A comprehensive rocket and radar study of midlatitude spread F. *J Geophys Res* **115**: A12339. DOI:1029/2010JA015503.

Evans JV, Holt JM, Wand RH. 1983. A differential-Doppler study of traveling ionospheric disturbances from Millstone Hill. *Radio Sci* **18**: 435–451.

Fejer BG, Kelley MC. 1980. Ionospheric irregularities. *Rev Geophys* **18**: 401–454.

Fukao S, Kelley MC, Shirakawa T, Takami T, Yamamoto M, Tsuda T, Kato S. 1991. Turbulent upwelling of the mid-latitude ionosphere: 1. Observational results by the MU radar. *J Geophys Res* **96**: 3725–3746.

Haldoupis C, Kelley MC, Hussey GC, Shalimov S. 2003. Role of unstable sporadic-E layers in the generation of midlatitude spread F. *J Geophys Res* **108**: 2. DOI:10.1029/2003JA009956.

Hajkowicz LA. 2007. Morphology of quantified ionospheric range spread-F over a wide range of midlatitudes in the Australian longitudinal sector. *Ann Geophys* **25**: 1125–1130.

Hajkowicz LA. 2016. Effect of auroral substorms on the ionospheric range spread-F enhancements at high southern midlatitudes using real time vertical-sounding ionograms. *J Atmos Sol Terr Phys* **140**: 108–113.

Hanson WB, Sanatani S. 1973. Large NI gradients below the equatorial F peak. *J Geophys Res* **78**: 1167–1173.

Herman JR. 1966. Spread F and ionospheric F-region irregularities. *Rev Geophys* **4**: 255–299.

Hines CO. 1960. Internal atmospheric gravity waves at ionospheric heights. *Can J Phys* **38**: 1441–1481.

Hines CO. 1963. The upper atmosphere in motion. *Q J Royal Meteorol Soc* **89**: 1–42.

Huang CS, Miller CA, Kelley MC. 1994. Basic properties and gravity wave initiation of the midlatitude F region instability. *Radio Sci* **29**: 395–405. DOI:10.1029/93RS01669.

Huang CY, Marcos FA, Roddy PA, Hairston MR, Coley WR, Roth C, Bruinsma S, Hunton DE. 2009. Broad plasma decreases in the equatorial ionosphere. *Geophys Res Lett* **36**. DOI:10.1029/2009GL039423.

Huang WQ, Xiao Z, Xiao SG, Zhang DH, Hao YQ, Suo YC. 2011. Case study of apparent longitudinal differences of spread F occurrence for two midlatitude stations. *Radio Sci* **46**. DOI:10.1029/2009RS004327.

Igarashi K, Kato H. 1993. Solar cycle variations and latitudinal dependence on the midlatitude spread F occurrence around Japan. Paper presented at the XXIV General Assembly. Kyoto, Japan: Int. Union of Radio Sci.

Jayachandran B, Balan N, Nampoothiri SP, Rao PB. 1987. HF Doppler observations of vertical plasma drifts in the evening F region at the equator. *J Geophys Res* **92**: 11253–11256.

Kelly MC. 1989. The Earth's ionosphere. *Int Geophys Ser* **43**: 71.

Kelley MC, Fukao S. 1991. Turbulent upwelling of the midlatitude ionosphere 2. Theoretical framework. *J Geophys Res* **96**: 3747–3753.

Kelley MC, Haerendal G, Kappler H, Valenzuela A, Balsley BB, Carter DA, Ecklund WL, Carlson CW, Hausler B, Torbert R. 1976. Evidence for a Rayleigh-Taylor type instability and upwelling of depleted densityregions during equatorial spread F. *Geophys Res Lett* **3**: 448–450.

King GAM. 1970. Spread-F on ionograms. *J Atmos Terr Phys* **32**: 209–212.

Kotake N, Otsuka Y, Tsugawa T, Ogawa T, Saito A. 2006. Climatological study of GPS total electron content variations caused by medium-scale traveling ionospheric disturbances. *J Geophys Res* **111**. DOI:10.1029/2005JA011418.

Lambert S. 1988. Frequency and duration of disturbances in the mid-latitude F region of the ionosphere. *Radio Sci* **23**: 693–707.

Lee CC, Chen WS. 2015. Effects of sporadic E-layer characteristics on spread-F generation in the nighttime ionosphere near a northern equatorial anomaly crest during solar minimum. *J Atmos Sol Terr Phys* **128**: 33–39.

Li G, Ning B, Abdu M, Yue X, Liu L, Wan W, Hu L. 2011. On the occurrence of postmidnight equatorial F region irregularities during the June solstice. *J Geophys Res* **116**: A04318. DOI:10.1029/2010JA016056.

Liu L, Wan W, Ning B, Pirog OM, Kurkin VI. 2006. Solar activity variations of the ionospheric electron density. *J Geophys Res* **111**: A08304. DOI: 10.1029/2006JA011598.

Lyon AJ, Skinner NJ, Wright RW. 1961. Equatorial spread-F at Ibadan, Nigeria. *J Atmos Terr Phys* **21**: 101–119.

Mathews JD, Gonzalez S, Sulzer MP, Zhou Q-H, Urbina J, Kudeki E, Franke S. 2001. Kilometer-scale layered structures inside spread-F. *Geophys Res Lett* **28**: 4167–4170.

McClure JP, Hanson WB, Hoffman JH. 1977. Plasma bubbles and irregularities in the equatorial ionosphere. *J Geophys Res* **82**: 2650–2656.

McNicol RWE, Webster HC, Bowman GG. 1956. A Study of Spread-F Ionospheric Echoes at Night at Brisbane. I. Range Spreading (Experimental). *Aust J Phys* **9**: 247–271.

Mwene AM, Earle GD, McClure PJ. 2004. Seasonal and longitudinal variations of midlatitude topside spread echoes based on ISS-b observations. AGU Fall Meeting Abstracts

Oikonomou C, Haralambous H, Haldoupis C, Meek C. 2014. Sporadic E tidal variabilities observed with the Cyprus Digisonde. *J Atmos Terr Phys* **119**: 173–183.

Otsuka Y, Shiokawa K, Ogawa T, Yokoyama T, Yamamoto M. 2009. Spatial relationship of nighttime medium-scale traveling ionospheric disturbances and F region field-aligned irregularities observed with two spaced all-sky airglow imagers and the middle and upper atmosphere radar. *J Geophys Res* **114**. DOI: 10.1029/2008JA013902.

Perkins FW. 1973. Spread F and ionospheric currents. *J Geophys Res* **78**: 218–226.

Rastogi RG. 1977. Equatorial range spread F and high multiple echoes from the F region. *Proc Ind Acad Sci Sect A* **85**: 230–235.

Rastogi RG, Klobuchar JA. 1990. Ionospheric electron content within the equatorial F2 layer anomaly belt. *J Geophys Res* **95**: 19045–19052.

Reinisch BW, Galkin IA, Khmyrov GM. 2009. The new digisonde for research and monitoring applications. *Radio Sci* **44**: RS0A24. DOI:10.1029/2008RS004115.

Shimazaki T. 1962. A statistical study of occurrence probability of spread F at high latitudes. *J Geophys Res* **67**: 4617–4634.

Shiokawa K, Ihara C, Otsuka Y, Ogawa T. 2003. Statistical study of nighttime medium-scale traveling ionospheric disturbances using midlatitude airglow images. *J Geophys Res* **108**. DOI:10.1029/2002JA009491.

Singleton DG. 1957. A Study of Spread F ionospheric echoes at night at Brisbane. III. Frequency spreading. *Aust J Phys* **10**: 60–76.

Singleton DG. 1968. The morphology of spread-F occurrence over half a sunspot cycle. *J Geophys Res* **73**: 295–308.

Swartz WE, Collins SC, Kelley MC, Makela JJ, Kudeki E, Franke S, Urbina J. 2002. First observations of an F-region turbulent upwelling coincident with severe E-region plasma and neutral atmosphere perturbations. *J Atmos Sol Terr Phys* **64**: 1545–1556.

Tsunoda RT. 2008. Satellite traces: an ionogram signature for large-scale wave structure and a precursor for equatorial spread F. *Geophys Res Lett* **35**. DOI:10.1029/2008GL035706.

Tsunoda RT. 2009. Multi-reflected echoes: another ionogram signature of large-scale wave structure. *Geophys Res Lett* **36**. DOI:10.1029/2008GL036221.

Tsunoda RT, Towle DM. 1979. On the spatial relationship of 1-meter equatorial spread-F irregularities and depletions in total electron content. *Geophys Res Lett* **6**: 873–876.

Tsunoda RT, White BR. 1981. On the generation and growth of equatorial backscatter plumes 1. Wave structure in the bottomside F layer. *J Geophys Res* **86**: 3610–3616.

Tsunoda RT, Cosgrove RB. 2001. Coupled electrodynamics in the nighttimemidlatitude ionosphere. *Geophys Res Lett* **28**: 4171–4174. DOI:10.1029/2001GL013245.

Tsunoda RT, Ecklund WL. 2007. On the post-sunset rise of the equatorial F layer and superposed upwellings and bubbles. *Geophys Res Lett* **34**. DOI:10.1029/2006GL028832.

Upadhayaya AK, Gupta S. 2014. A statistical analysis of occurrence characteristics of Spread-F irregularities over Indian region. *J Atmos Sol Terr Phys* **112**: 1–9.

Verhulst T, Altadill D, Mielich J, Reinisch B, Galkin I, Mouzakis A, Belehaki A, Buresova D, Stanimir S, Blanch E, Kouba D. 2017. Vertical and oblique HF sounding with a network of synchronize dionosondes. *Adv Space Res*. DOI:10.101/j.asr.2017.06.033. (in press).

Wang GJ, Shi JK, Wang X, Shang S-P., Zherebtsov G, Pirog OM. 2010. The statistical properties of spread F observed at Hainan station during the declining period of the 23rd solar cycle. *Ann Geophys* **28**: 1263–1271.

Weber EJ, Buchau J, Moore JG. 1980. Airborne studies of equatorial F layer ionospheric irregularities. *J Geophys Res* **85**: 4621–4641.

Woodman RF, La Hoz C. 1976. Radar observations of F region equatorial irregularities. *J Geophys Res* **81**: 5447–5466.

Xiao Z, Xiao S, Hao Y, Zhang D. 2007. Morphological features of ionospheric response to typhoon. *J Geophys Res* **112**. DOI:10.1029/2006JA011671.

Xiao SG, Xiao Z, Shi JK, Zhang DH, Feng XS, Hao YQ, Huang WQ. 2009. Observational facts in revealing a close relation between acousticgravity waves and midlatitude spread F. *J Geophys Res* **114**: A01303. DOI:10.1029/2008JA013747.

Yokoyama T, Hysell DL, Otsuka Y, Yamamoto M. 2009. Three-dimensional simulation of the coupled Perkins and Es-layer instabilities in the nighttime midlatitude ionosphere. *J Geophys Res* **114**. DOI:10.1029/2008JA013789.

Zhang Y, Wan W, Li G, Liu L, Hu L, Ning B. 2015. A comparative study of GPS ionospheric scintillations and ionogram spread F over Sanya. *Ann Geophys* **33**: 1421–1430.

Cite this article as: Paul KS, Haralambous H, Oikonomou C, Paul A, Belehaki A, Ioanna T, Kouba D, Buresova D. 2018. Multi-station investigation of spread F over Europe during low to high solar activity. *J. Space Weather Space Clim.* **8**: A27.